HHS Public Access

Author manuscript

Cell Rep. Author manuscript; available in PMC 2021 September 12.

Published in final edited form as:

Cell Rep. 2021 August 24; 36(8): 109603. doi:10.1016/j.celrep.2021.109603.

NKD2 mediates stimulation-dependent ORAI1 trafficking to augment Ca^{2+} entry in T cells

Beibei Wu[1], **Jin Seok Woo**[1], **Pamela Vila**[1,4], **Marcus Jew**[1,5], **Jennifer Leung**[1,6], **Zuoming Sun**[2], **Sonal Srikanth**[1,3,7,*], **Yousang Gwack**[1,3,*]

[1]Department of Physiology, David Geffen School of Medicine, University of California, Los Angeles, Los Angeles CA 90095, USA

[2]Department of Molecular Imaging & Therapy, Beckman Research Institute of City of Hope, Duarte, CA 91010, USA

[3]Senior author

[4]Present address: Olive View-UCLA Medical Center, 14445 Olive View Drive, Sylmar, CA 91342, USA

[5]Present address: Ronald Reagan UCLA Medical Center, 757 Westwood Plaza, Los Angeles, CA 90095, USA

[6]Present address: Department of Biomedical Sciences, Cedars-Sinai Medical Center, Los Angeles, CA 90048, USA

[7]Lead contact

SUMMARY

Sustained activation of the Ca^{2+}-release-activated Ca^{2+} (CRAC) channel is pivotal for effector T cell responses. The mechanisms underlying this sustainability remain poorly understood. We find that plasma membrane localization of ORAI1, the pore subunit of CRAC channels, is limited in effector T cells, with a significant fraction trapped in intracellular vesicles. From a targeted screen, we identify an essential component of $ORAI1^{+}$ vesicles, naked cuticle homolog 2 (NKD2). Mechanistically, NKD2, an adaptor molecule activated by signaling pathways downstream of T cell receptors, orchestrates trafficking and insertion of ORAI1 + vesicles to the plasma membrane. Together, our findings suggest that T cell receptor (TCR)-stimulation-dependent

*Correspondence: ssrikanth@mednet.ucla.edu (S.S.), ygwack@mednet.ucla.edu (Y.G.).

AUTHOR CONTRIBUTIONS

Y.G. and S.S. designed and supervised the research. S.S. supervised generation of the cDNA library and performed the cDNA screen and most of the Ca^{2+} imaging, confocal (with B.B.W.), and TIRF microscopy experiments. B.B.W. performed most of the biochemistry and flow cytometry experiments with help from J.S.W. P.V. and M.J. helped in cloning the cDNAs. J.L. helped with the subcloning of NKD2 into different vectors. Z.S. provided reagents for PKC clones and advice on manuscript preparation. Y.G., S.S., and B.B.W. wrote the manuscript.

DECLARATION OF INTERESTS

The authors declare no competing interests.

SUPPLEMENTAL INFORMATION

Supplemental information can be found online at https://doi.org/10.1016/j.celrep.2021.109603.

insertion of ORAI1 into the plasma membrane is essential for sustained Ca^{2+} signaling and cytokine production in T cells.

Graphical abstract

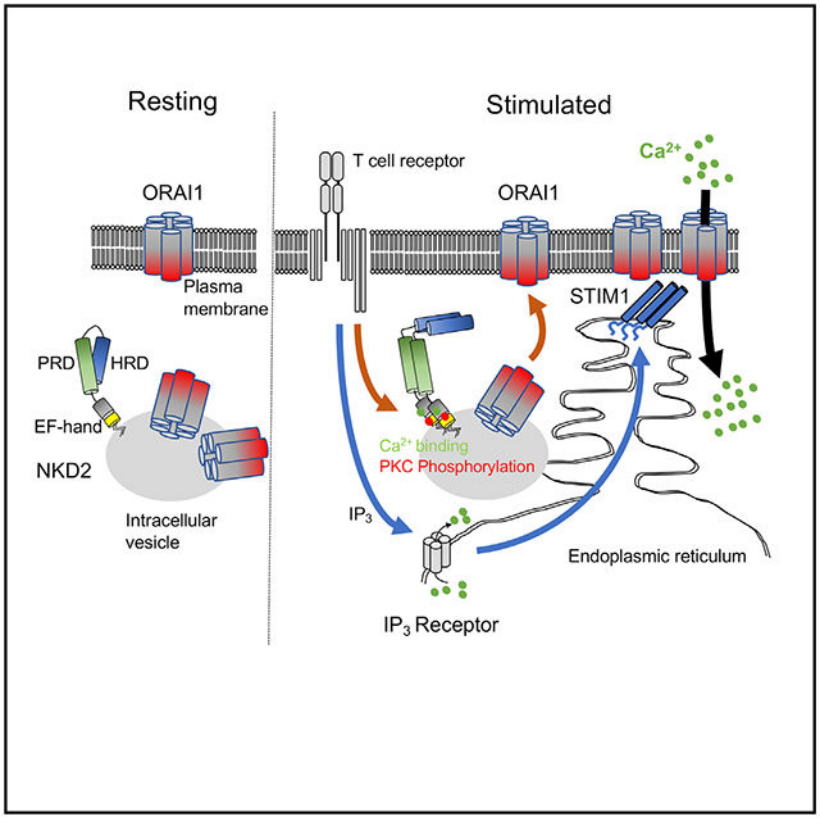

In brief

Wu et al. address the mechanism underlying sustained activation of the Ca^{2+}-release-activated Ca^{2+} (CRAC) channel that is pivotal for effector T cell responses. They report that NKD2-mediated insertion of ORAI1 into the plasma membrane after TCR stimulation is essential for sustained Ca^{2+} signaling and cytokine production in T cells.

INTRODUCTION

Ca^{2+} signaling in T cells is primarily mediated by store-operated Ca^{2+} entry (SOCE) induced by depletion of the endoplasmic reticulum (ER) Ca^{2+} stores after engagement of T cell receptors with cognate antigens. A specialized class of store-operated Ca^{2+} (SOC) channels, Ca^{2+}-release-activated Ca^{2+} (CRAC) channels, play a major role in elevation of intracellular Ca^{2+} concentration ($[Ca^{2+}]$) in T cells (Lewis, 2011; Srikanth and Gwack, 2013). CRAC channels consist of two major components: the plasma membrane (PM)-localized pore subunit ORAI1 and an ER-resident Ca^{2+} sensor, stromal interaction molecule 1 (STIM1). STIM1 senses depletion of the ER Ca^{2+} stores and interacts with ORAI1 to open the pore. High and sustained Ca^{2+} signaling mediated by CRAC channels is

essential for the induction of transcriptional programs via the NFAT (nuclear factor of activated T cells) pathway (Lewis, 2011; Srikanth and Gwack, 2013). Severe combined immunodeficiency (SCID) caused by mutations in *ORAI1* or *STIM1* and the widespread use of inhibitors of this pathway, cyclosporine A and FK506 in clinics, underscore the importance of therapeutic targeting of the Ca^{2+}-NFAT pathway (Feske et al., 2015; Srikanth and Gwack, 2013). However, inhibition of the core subunits of CRAC channels, ORAI1 and STIM1, can have pleiotropic effects due to their ubiquitous expression, impeding the therapeutic exploitation of this pathway. Therefore, it is important to identify cell-type-specific mechanisms underlying the regulation of CRAC channels for the design of targeted therapeutic strategies.

Among the multiple models for CRAC channel activation that were initially proposed, three models were extensively pursued experimentally. These included conformational coupling, a diffusible messenger, and exocytosis models (Parekh and Penner, 1997; Parekh and Putney, 2005; Putney et al., 2001). The conformational coupling model involves direct interaction between Ca^{2+} sensor protein(s) localized on the ER membrane and the CRAC channel on the PM, such that ER store depletion would alter ER-resident proteins' conformation to allow their interaction with the CRAC channels (Irvine, 1990). Originally, the ER-resident inositol 1,4,5-trisphosphate receptor ($InsP_3R$) was proposed to act as the Ca^{2+} sensor in the ER and the inositol 1,3,4,5-tetrakisphosphate receptor ($InsP_4R$) as the CRAC channel in the PM (Irvine, 1990). The diffusible messenger model suggests the release of a diffusible activating factor from the ER, called the calcium influx factor (CIF) after store depletion, which would then activate the PM-resident CRAC channels (Randriamampita and Tsien, 1993). Finally, the exocytosis model posits that active CRAC channels are inserted into the PM by vesicle fusion in response to store depletion (Fasolato et al., 1993). The characterization of the STIM-ORAI coupling mechanism primarily supports the conformational coupling model; however, the molecular components are different from those originally proposed (Prakriya and Lewis, 2015). These studies have resulted in the neglection of the experimental evidence supporting the other models of SOCE activation. For example, brefeldin A and primaquine that block vesicular transport suppressed SOCE (Gregory and Barritt, 1996; Somasundaram et al., 1995; Yao et al., 1999). SOCE also depends on the function of an essential component of vesicle fusion, soluble N-ethylmaleimide-sensitive factor attachment protein receptor (SNARE) (Alderton et al., 2000; Woodard et al., 2008; Yao et al., 1999). Furthermore, a recent report suggested that a vast majority of ORAI1 protein (60%) was localized in intracellular recycling vesicles, and this pool trafficked to the PM after the elevation of $[Ca^{2+}]$ (Hodeify et al., 2015). Based on these observations, the intracellular ORAI1 pool may significantly contribute to CRAC channel activation; however, its physiological role and the signals involved in vesicular trafficking remain unknown.

In this study, we have identified naked cuticle homolog 2 (NKD2), a component of intracellular vesicles, as a vital regulator of CRAC channels that mediates trafficking of intracellular $ORAI1^+$ vesicles to the PM in effector T cells. Our data show that T cell receptor (TCR) stimulation induces the insertion of $ORAI1^+$ vesicles into the PM in an NKD2-dependent manner. Using pH-sensitive GFP-tagged ORAI1, we show insertion of $ORAI1^+$ vesicles to the PM in a TCR-stimulation-dependent manner, which was profoundly

impaired in NKD2-deficient cells. Furthermore, NKD2-mediated insertion of intracellular ORAI1 to the PM was dependent on protein kinase C (PKC) and Ca^{2+} signaling pathways. Deletion of NKD2 impaired surface insertion of $ORAI1^{+}$ vesicles, SOCE, and cytokine production in primary human T cells. Our results show that SOCE in effector T cells is sustained by replenishing PM-resident ORAI1 pool from intracellular vesicles.

RESULTS

Identification of NKD2 as a regulator of the Ca^{2+}-NFAT pathway in T cells

Human Genome Organization (HUGO) database shows that approximately 200 proteins containing single or multiple Ca^{2+}-binding EF-hand motifs may act as Ca^{2+} sensors or buffers. To check their potential role in regulation of CRAC channels, we generated an expression library in a retroviral vector containing cytomegalovirus (CMV) promoter-cDNA-FLAG taginternal ribosome entry site (IRES)-EGFP for both transient transfection and retroviral transduction purposes (Table S1). SOCE and intracellular localization were examined in cells expressing individual candidates (Figures S1A and S1B). From this targeted low-throughput screen using single-cell Ca^{2+} imaging, we identified NKD2 as a novel regulator of CRAC channels. Interestingly, we found that Nkd, the *Drosophila* homolog of NKD2, was one of the candidates from our previous genome-wide RNAi screen using *Drosophila* cells to identify regulators of the Ca^{2+}-NFAT pathway (Gwack et al., 2006). Identification of NKD2 from two independent unbiased screens suggested its important role in regulation of the CRAC channels.

Immunoblot analysis showed abundant expression of NKD2 proteins in Jurkat T cells, whereas it was almost undetectable in HeLa cells (Figure 1A). This result was consistent with the previous finding that *NKD2* mRNA was upregulated in another leukemic cell line, MOLT-4, compared with other cancer cell lines (Katoh, 2001). We also observed that the molecular weight (MW) of NKD2 in T cells stimulated with a combination of phorbol 12-myristate 13-acetate (PMA) and ionomycin or anti-CD3 antibody cross-linking was slightly higher than under resting conditions, suggesting a stimulation-induced posttranslational modification. To examine the role of NKD2 in T cells, we generated NKD2 knockout (KO) Jurkat T cells using the CRISPR-Cas9 system with two independent single guide RNAs (sgRNAs), followed by clonal selection (Figure 1B). SOCE triggered by TCR stimulation was substantially reduced in NKD2 KO Jurkat cells (Figure 1C). After 10 min of TCR stimulation, cells were treated with an ionophore, ionomycin, that almost completely depletes the ER Ca^{2+} stores, to determine the maximal SOCE levels. Ionomycin-induced SOCE was also impaired in NKD2 KO cells, which was rescued by reconstitution of NKD2 expression. SOCE induced by passive depletion of the intracellular stores with thapsigargin (TG), a blocker for the sarco/ER ATPase (SERCA) pump, was also impaired in NKD2 KO Jurkat T cells, albeit to a lesser degree (Figure S1C). However, the basal and ER Ca^{2+} levels were not significantly changed in NKD2 KO cells (Figure S1D).

A crucial role of ORAI1 in activation of the Ca^{2+}-NFAT signaling pathway is well established (Kim et al., 2011). Previously, we showed that dephosphorylation/nuclear translocation of NFATc2 and induction of NFATc1 were excellent readouts for the short- and long-term effects of Ca^{2+} entry, respectively (Kim et al., 2011, 2014). Immunoblotting

showed that nuclear translocation of NFATc2 and induction of NFATc1 were profoundly decreased in NKD2 KO cells compared with control cells (Figures 1D and 1E). Impaired NFAT activation in NKD2 KO cells resulted in a substantial reduction in interleukin-2 (IL-2) expression, which was recovered by reconstitution with NKD2 (Figure 1F). In addition to Ca^{2+} signaling, we also checked the potential role of NKD2 in other proximal TCR and co-receptor signaling pathways, including the extracellular signal-related kinase (ERK), p38, c-Jun N-terminal kinase (JNK), nuclear factor κB (NF-κB), protein kinase B (PKB [or AKT]), and mTOR pathways, but these pathways were unaffected in NKD2 KO Jurkat T cells (Figures S2A and S2B). NKD2 was originally identified as an inhibitor for the Wnt/β-catenin pathway; hence, we examined this pathway after TCR stimulation (Dong et al., 2015; Zeng et al., 2000; Zhao et al., 2015). While TCR stimulation enhanced the protein levels of β-catenin, we did not observe any difference between control and NKD2 KO Jurkat T cells. Finally, immunoblot analysis showed that expression of critical components of the CRAC channels, ORAI1 and STIM1, as well as PM Ca^{2+} ATPase 4 (PMCA4), an important regulator for Ca^{2+} exclusion and influx in T cells (Ritchie et al., 2012), were not influenced by NKD2 deficiency (Figure S2C). Together, these data show an essential and selective role of NKD2 in regulation of Ca^{2+} signaling in T cells.

NDK2 mediates trafficking of intracellular ORAI1^{+} vesicles to the PM after TCR stimulation

NKD2 was identified as an inhibitor for the Wnt/β-catenin pathway and a component of vesicles for the secretion of transforming growth factor α (TGF-α) (Dong et al., 2015; Li et al., 2004; Zeng et al., 2000; Zhao et al., 2015). To elucidate the mechanism underlying its involvement in SOCE, we checked intracellular localization of NKD2 together with ORAI1. In Jurkat T cells, NKD2 was localized in intracellular vesicles (Figure 2A). Interestingly, we also observed a significant fraction of ORAI1 localized to intracellular vesicles. Importantly, a majority of intracellular ORAI1^{+} vesicles (>75%) were also positive for NKD2 (Figure 2A, top two panels; Pearson's correlation coefficient, 0.83 ± 0.006). Upon stimulation on anti-CD3 antibody-coated coverslips, Jurkat T cells showed enhanced accumulation of ORAI1/NKD2^{+} vesicles at the interface between the T cell and the stimulatory surface (Figure 2A, bottom three panels).

ORAI1 is recruited to the immunological synapse (IS), and this recruitment is vital for local, high [Ca^{2+}] that influences the charge properties of phospholipids for amplification of TCR signals (Lioudyno et al., 2008; Shi et al., 2013). However, the current ORAI1-STIM1 coupling model cannot explain the polarized accumulation of ORAI1 because the ER-PM junctions are evenly distributed throughout the periphery of the cell. We hypothesized that one of the mechanisms underlying the polarized accumulation of ORAI1 might be mediated by vesicle trafficking directed to the IS. To check this possibility, we examined whether ORAI1/NKD2^{+} vesicles accumulated at the IS. Confocal microscopy analysis showed polarized accumulation of ORAI1/NKD2^{+} vesicles at the IS formed between T cells and superantigen-pulsed antigen-presenting cells (APCs) (Figure 2B). Furthermore, using real-time live-cell total internal reflection fluorescence (TIRF) microscopy, we observed accumulation of ORAI1/NKD2^{+} vesicles at the interface between Jurkat T cells and anti-CD3 antibody-coated coverslips (Figure 2C). Our results suggest that in addition to PM-

localized ORAI1, the intracellular source of ORAI1 from vesicles may enhance and sustain SOCE in T cells.

We further investigated whether intracellular ORAI1 is indeed inserted into the PM using an antibody recognizing the extracellular domain of ORAI1. First, by performing ORAI1 staining in permeabilized cells, we confirmed that the total amount of endogenous ORAI1 proteins in control and NKD2 KO Jurkat cells was similar (Figure 3A), in agreement with our prior immunoblotting results (Figure S2C). In this analysis, we used ORAI1 KO Jurkat T cells generated using the CRISPR-Cas9 system to validate specificity of anti-ORAI1 antibody. Next, using this antibody, we checked the levels of surface ORAI1 in non-permeabilized Jurkat T cells before and after TCR stimulation. To accurately estimate the contribution of NKD2 in trafficking of ORAI1 after TCR stimulation, we first masked the PM-resident ORAI1 protein using saturating concentrations of anti-ORAI1 antibody. Subsequently, these cells were stimulated with anti-CD3 antibodies, and newly integrated ORAI1 was stained with fluorescence-conjugated anti-ORAI1 antibody (Figure 3B). Using this method, we validated an increase of surface ORAI1 after TCR stimulation that was profoundly reduced in NKD2 KO Jurkat T cells. These results validate a critical role for NKD2 in surface insertion of ORAI1 upon TCR stimulation.

In addition to analysis of endogenous ORAI1 protein, we took advantage of a dually tagged ORAI1 reporter with EGFP at the N terminus and a hemagglutinin (HA) tag inserted in its second extracellular loop (GFP-ORAI1-EC-HA) (Figure 3C). It is a useful reporter because GFP allows for gating of the cells with similar ORAI1 expression, whereas surface staining with anti-HA antibodies permits selective detection of PM-resident ORAI1 (Figures S3A and S3B). To specifically detect cells showing enhanced surface ORAI1 levels upon TCR stimulation, we gated on ORAI1^{high} population, which was similar between control and NKD2 KO T cells under resting conditions (Figures 3D and 3E). Consistent with microscopy and flow cytometric analysis of endogenous ORAI1, we observed that surface expression of ORAI1 increased upon TCR stimulation (peaked at 20 min), which was reduced by the deficiency of NKD2. We also confirmed that reconstitution of NKD2 expression in those KO cells recovered the surface expression of ORAI1. In support of our flow cytometry and endogenous SOCE measurements, NKD2 KO Jurkat T cells expressing GFP-ORAI1-EC-HA also showed severe reduction in SOCE, compared with control cells, especially sustained levels of SOCE (Figure 3F). These results suggest that NKD2-mediated trafficking of ORAI1^{+} vesicles is especially essential to maintain the sustained levels of SOCE after TCR stimulation by providing an additional source for ORAI1 from the intracellular pool.

Visualization of ORAI1^{+} vesicle trafficking using a pH-sensitive biomarker

To gain an in-depth insight into the mechanism and kinetics of trafficking and membrane integration of ORAI1^{+} vesicles, we generated an ORAI1 construct that contains a pH-sensitive GFP variant biomarker, pHluorin, in the second extracellular domain (Wienisch and Klingauf, 2006). The pHluorin sensor is non-fluorescent in an acidic environment with a pH of ≤5.6 (e.g., the lumen of endocytic vesicles), but becomes fluorescent under neutral or alkaline conditions (pKa of ~7.1) (Miesenböck et al., 1998). We also incorporated two

tobacco etch virus (TEV) protease cleavage sites flanking pHluorin to remove background signals from pre-existing ORAI1 in the PM by treatment with TEV protease. To provide better accessibility to TEV protease, we used the ORAI1^{N223A} mutant, which is not glycosylated in its extracellular loop region but is functionally active (Gwack et al., 2007), to generate ORAI1^{N223A}-EC-TEV-pHluorin-TEV. We performed several control experiments to validate the usefulness of this biomarker. First, we validated its pH sensitivity. In resting cells, we could detect GFP signals from only the PM, and this signal was lost when the pH of the extracellular solution was changed to acidic (Figure 4A). By contrast, alkalinization of the intracellular milieu by adding NH_4Cl in the external solution enhanced the fluorescence intensity and allowed for detection of intracellular ORAI1. Next, we checked the accessibility of TEV protease cleavage sites and observed that treatment with TEV protease for ~15 min reduced fluorescence of PM-resident ORAI1 by more than 70% (Figure 4B).

Using ORAI1^{N223A}-EC-TEV-pHluorin-TEV, we examined the membrane integration of ORAI1 using flow cytometry and microscopy. Without TEV cleavage, we observed an approximately 2-fold increase in pHluorin^{high} population in control cells after TCR stimulation, which was dampened in NKD2 KO Jurkat T cells (Figure 4C, left two panels). TEV treatment reduced the background fluorescence from PM-resident ORAI1. We observed a more than 5-fold increase in pHluorin^{high} population in control cells after TCR stimulation, which was decreased dramatically in NKD2 KO cells (Figure 4C, right two panels and bar graph). To visualize ORAI1^{+} vesicles' insertion upon TCR stimulation, we dropped TEV-protease-treated control or NKD2 KO Jurkat T cells expressing ORAI1^{N223A}-EC-TEV-pHluorin-TEV on stimulatory anti-CD3 antibody-coated coverslips and examined PM proximal events using TIRF microscopy. Because of TEV treatment, the background fluorescence from PM-resident ORAI1 was minimal. As the control cells started spreading, we observed distinct fluorescence spots on the PM due to the fusion of ORAI1^{+} vesicles to the PM (Figure 4D). The kinetics of ORAI1^{+} vesicle fusion examined by TIRF microscopy showed a slow and dynamic process occurring over the time frame of minutes, similar to our observations with flow cytometry measurements. We quantified each spot as a distinct vesicle fusion event and observed a profound reduction in the fluorescence intensity and number of vesicles inserted in NKD2 KO Jurkat T cells. These results validate the PM insertion of ORAI1^{+} vesicles upon TCR stimulation in Jurkat T cells and the crucial role of NKD2 in this process.

PKC-mediated phosphorylation of NKD2

The human genome database shows two different splice isoforms of *NKD2* encoding proteins of 451 and 311 amino acids that differ in their C-terminal sequences (Figure S4A). Immunoblotting with an antibody targeting the conserved N terminus of NKD2 detected a single band of ~55 kDa corresponding to the longer isoform in T cells (Figure 1A; Figure S2C). Hence, we used a cDNA corresponding to the longer isoform for all our expression and biochemical analyses. NKD2 has a myristoylation site (glycine) and positively charged residues in its N terminus for phospholipid binding (Figure 5A) (Li et al., 2004, 2007). It also contains a Ca^{2+}-sensing EF-hand motif in the N terminus and proline- and histidine-rich domains in the C terminus. The EF-hand and proline-rich domains bind

to Dishevelled (Dvl), a signaling adaptor for the Wnt/β-catenin pathway, and TGF-α for its secretion, respectively (Li et al., 2004, 2007; Rousset et al., 2002). Because of its capacity to interact directly with cargo (Li et al., 2007), we examined whether NKD2 interacts with ORAI1 using co-immunoprecipitation, but failed to detect any interaction between the two proteins (Figure S4B). Furthermore, bacterially expressed glutathione S-transferase (GST)-fused fragments of NKD2 did not pull down full-length ORAI1 (Figure S4C). These experiments suggest that NKD2 may not be directly involved in selecting ORAI1 as a cargo protein.

Since we could not detect any interaction between NKD2 and ORAI1, we hypothesized that NKD2 acts as a signaling adaptor and transmits TCR signals to effector molecules for trafficking of ORAI1$^+$ vesicles. TCR signal activates phospholipase C-γ1 (PLCγ1) that hydrolyzes phosphatidylinositol 4,5-bisphosphate (PIP_2) into $InsP_3$ and diacylglycerol (DAG) (Hogan et al., 2003; Srikanth and Gwack, 2013). $InsP_3$ binds to the $InsP_3R$ to deplete the ER Ca^{2+} stores and activate CRAC channels, while DAG binds to PKC and activates downstream mitogen-activated protein kinase (MAPK)-activator protein 1 (AP1) and NF-κB pathways. To activate the TCR downstream MAPK-AP1 and Ca^{2+} signaling pathways, we treated Jurkat T cells with a DAG homolog, PMA, and ionomycin. We found an increase in the molecular weight of NKD2 in PMA-treated cells, but not in those treated with ionomycin, suggesting possible PKC-mediated phosphorylation of NKD2 (Figure 5B, left panel). PKC-θ plays an essential role in T cell activation among PKC family members, especially in sustaining TCR signals, after being recruited into the IS (Coudronniere et al., 2000; Lin et al., 2000; Quann et al., 2011; Sun et al., 2000). Also, earlier reports have shown PKC-θ-mediated augmentation of SOCE in T cells (Altman et al., 2004; Pfeifhofer et al., 2003), but the underlying molecular mechanism remains unknown. To examine whether PKC-θ can phosphorylate NKD2, we examined NKD2 modification in HEK293T cells overexpressing the wild-type (WT), the constitutive active (CA), and the dominant-negative (DN) mutants of PKC-θ (Kwon et al., 2012; Ma et al., 2012) together with NKD2. Immunoblotting showed a higher molecular weight band for NKD2 in cells co-expressing the CA mutant, but not WT PKC-θ or its DN mutant (Figure 5B, right). Bioinformatics tools, including MotifScan, identified three residues (S31, S230, and T257) within NKD2 as potential PKC-mediated phosphorylation sites. Hence, we generated S31A, S230A, and T257A mutants of NKD2 and coexpressed them with CA PKC-θ to examine their phosphorylation by immunoblotting with anti-NKD2 antibody as well as a phospho-serine-specific antibody (Figure 5C). These results identified the S31 residue as a PKC-θ-mediated phosphorylation site in NKD2. Interestingly, we found that PKC-θ-mediated phosphorylation significantly induced homo-multimerization of NKD2, which was abolished by the S31A substitution (Figure S4D), suggesting a potential role of phosphorylation in the active state of NKD2.

T cell receptor signals trigger NKD2-mediated ORAI1$^+$ vesicle trafficking

Based on the new finding of PKC-θ-mediated phosphorylation of NKD2, we examined the role of the functional domains of NKD2 in trafficking of ORAI1$^+$ vesicles. More specifically, to explore the role of myristoylation, Ca^{2+} binding via the EF-hand motif (Li et al., 2004, 2007), and PKC-θ-mediated phosphorylation in NKD2 (summarized in Figure

5A), we measured surface ORAI1 levels in NKD2 KO Jurkat T cells reconstituted with appropriate mutants of NKD2. We expressed $NKD2^{WT}$, $NKD2^{G2A}$, $NKD2^{132DFD134>AFA}$ (substitutions in positions 1 and 3 within the EF-hand loop), and $NKD2^{S31A}$ together with GFP-ORAI1-EC-HA in NKD2 KO Jurkat T cells. Compared with WT NKD2, all the mutants failed to enhance surface ORAI1 levels after TCR stimulation in NKD2 KO Jurkat T cells (Figure 5D). We also examined the sub-cellular localization of these mutants using confocal microscopy. Under resting conditions, $NKD2^{132DFD134>AFA}$ and $NKD2^{S31A}$ showed localization similar to $NKD2^{WT}$ and co-localized with $ORAI1^{+}$ vesicles, whereas $NKD2^{G2A}$ showed cytoplasmic localization and did not mark the $ORAI1^{+}$ vesicles (Figure 5E, top panels). As expected, upon TCR stimulation, cells expressing $NKD2^{WT}$ showed accumulation of $ORAI1^{+}$ vesicles at the interface between the T cell and the anti-CD3 antibody-coated coverslip. However, cells expressing either the $NKD2^{132DFD134>AFA}$ or $NKD2^{S31A}$ that showed co-localization of these mutants with $ORAI1^{+}$ vesicles under resting conditions failed to show accumulation of $ORAI1^{+}$ vesicles at the interface between the T cell and the anti-CD3 antibody-coated coverslip. $NKD2^{G2A}$ that did not show co-localization with $ORAI1^{+}$ vesicles also failed to induce accumulation of $ORAI1^{+}$ vesicles at the interface between the T cell and the anti-CD3 antibody-coated coverslip (Figure 5E, bottom panels), in support of our $ORAI1^{+}$ vesicle trafficking data (Figure 5D). SOCE measurements in NKD2 KO cells further supported these results, where none of the mutants reconstituted SOCE compared with WT NKD2 (Figure 5F). From these results, we conclude that myristoylation, Ca^{2+} binding, and PKC-θ-mediated phosphorylation of NKD2 are required for $ORAI1^{+}$ vesicle trafficking. While myristoylation was crucial for retaining NKD2 to the vesicles, TCR signals, including Ca^{2+} elevation and PKC-θ-mediated phosphorylation, played a direct role in $ORAI1^{+}$ vesicle trafficking. However, stimulation of Jurkat T cells with PMA, ionomycin, or both was not enough to induce trafficking of $ORAI1^{+}$ vesicles robustly, compared with TCR stimulation, suggesting the presence of additional mechanisms in this process (Figure S4E).

CD28 signaling plays a crucial role in T cell activation, proliferation, and survival and hence has been one of the targets of immunomodulatory therapeutics (Esensten et al., 2016; Zhang and Vignali, 2016). CD28 signaling augments PKC-θ and PLCγ1-Ca^{2+} signaling (Esensten et al., 2016; Tan et al., 2014). Consistent with these observations, we found that CD28 stimulation augmented TCR signaling-induced SOCE in Jurkat T cells, and this augmentation was abolished by NKD2 deficiency (Figure S5A). We also found that CD28 signaling alone can induce a minor, but statistically significant increase in ORAI1 surface expression, which was substantially reduced in NKD2 KO cells (Figure S5B). Under weak TCR stimulation with low concentrations of anti-CD3 antibody, the augmentation by CD28 signaling was more evident than strong TCR stimulation, and both showed dependence on NKD2 (Figure S5C). These results suggest that CD28 signaling acts synergistically with TCR signaling to enhance NKD2-mediated $ORAI1^{+}$ vesicle trafficking by augmenting the PKC-θ and Ca^{2+} signaling pathways.

Role of NKD2 in primary effector T cells

To examine whether NKD2 is crucial for the function of primary T cells, we differentiated human naive $CD4^{+}$ T cells to effector T cells after transduction with lentiviral vectors

encoding two independent sgRNAs targeting NKD2. We validated reduced NKD2 expression with both sgRNAs using intracellular staining and flow cytometry (Figure 6A). NKD2 KO primary T cells showed reduced SOCE after TCR cross-linking and ionomycin treatment (Figure 6B). Similar to our observations with Jurkat T cells, primary effector T cells also showed enhanced surface ORAI1 upon TCR stimulation, which was significantly reduced in *NKD2* KO effector T cells (Figure 6C). Furthermore, cytokine analysis showed reduced levels of interferon γ (IFN-γ), IL-2, and tumor necrosis factor (TNF) in *NKD2* KO effector T cells (Figure 6D). However, these decreases were limited to the effector function of T cells because NKD2 deficiency did not influence T-bet expression (Figure 6E) or proliferation of Jurkat and primary T cells (Figures S6A and S6B). Collectively, these analyses indicate an important role of NKD2 in the effector function of helper T cells.

DISCUSSION

Three models of CRAC channel activation were previously proposed: conformational coupling, diffusible messenger, and vesicle fusion models (Putney et al., 2001). The current paradigm of ORAI1-STIM1 interaction supports only the conformational coupling model, with little evidence for the other models. In *Xenopus* oocytes, internalization of ORAI1 through vesicle trafficking by Rab5, caveolin, and dynamin mediates inhibition of SOCE during meiosis (Yu et al., 2009, 2010). In widely used cell lines such as Chinese hamster ovary (CHO) and HEK293 cells, only ~40% of ORAI1 localizes to the PM, and enrichment of ORAI1 at the PM after store depletion is passively achieved by trapping recycling ORAI1 by STIM1 (Hodeify et al., 2015). However, it is currently unknown whether an active signaling mechanism exists to traffic ORAI1 from the intracellular pool to the PM. Using NKD2 as a molecular handle, we have identified a crucial role of $ORAI1^+$ vesicle trafficking, which is actively induced by TCR stimulation. Our findings bridge the conformational coupling and exocytosis models of CRAC channel activation, such that TCR-stimulation-induced transient conformational coupling-mediated activation of PM-resident ORAI1 channels allows for the fusion of intracellular $ORAI1^+$ vesicles to the PM to support sustained Ca^{2+} entry by establishing a positive feedback loop.

In this study, we focused on the role of NKD2 in T cells where the CRAC channel plays a predominant role in their effector functions, including cytokine production. A similar NKD2-mediated mechanism may also be utilized in other cell types. However, that would require simultaneous activation of multiple signaling pathways, maybe downstream of a G-protein-coupled receptor. In T cells, we observed abundant expression of NKD2 and simultaneous activation of multiple signaling pathways, including Ca^{2+} signaling itself and PKC-θ-mediated phosphorylation, upon TCR stimulation. We have also shown that co-receptor CD28 signaling augmented this activity. Other TCR signaling pathways may also play a role since chemical agonists of Ca^{2+} and PKC signaling pathways (i.e., PMA + ionomycin) induced less $ORAI1^+$ vesicle trafficking, compared with TCR stimulation. Our results show that individual activation of either the Ca^{2+}- or the PKC signaling pathways only induced 2- to 3-fold increase in the PM localization of ORAI1, compared with steady state, in consistence with previous observations (Woodard et al., 2008). Thus, it is likely that NKD2-mediated ORAI1 trafficking acts selectively in T cells because it requires a unique combination of Ca^{2+}- and PKC-dependent signals, and other unknown signaling pathways.

Our findings also suggest a possible mechanism underlying the polarized localization of ORAI1 at the IS (Lioudyno et al., 2008). The ORAI1-STIM1 coupling model cannot explain these proteins' preferential accumulation to the IS because the ER-PM junctions are scattered throughout the PM. Our data showing preferential trafficking of ORAI1-containing vesicles to these regions suggest that polarized activation of Ca^{2+} and PKC signaling in the IS (Barr et al., 2008; Lioudyno et al., 2008; Srikanth and Gwack, 2013; Zanin-Zhorov et al., 2011) may contribute to preferential accumulation of ORAI1 to these regions.

Here, we propose that NKD2 is a signaling adaptor molecule that is localized to $ORAI1^+$ vesicles under the steady state and transmits TCR signals to the effector molecules for vesicle trafficking (e.g., Rab GTPases). Considering that NKD2 deficiency did not significantly influence the basal surface levels of ORAI1, NKD2 seems to be primarily important for $ORAI1^+$ vesicle trafficking after TCR stimulation. If NKD2 acts as a signaling adaptor, we still do not understand which effector molecules are involved in this active process. Potential Rab GTPases as effector molecules in ORAI1 trafficking include Arf6/Rab4b/Rab11b (recycling vesicle), Rab29 (recycling vesicle and early secretion), Rab35 (early secretion), and Rab8b (late secretion). Especially in T cells, Rab4b mediates trafficking of vesicles containing the linker for activation of T cells (LAT) and TCRZ, while Rab11b is involved in trafficking of Lck (Choudhuri et al., 2014; Soares et al., 2013). Future studies using co-localization or loss-of-function approaches with candidate Rab GTPases will shed light on the effector molecules involved in $ORAI1^+$ vesicle trafficking. Our data suggest that intracellular $ORAI1^+$ vesicles indeed fuse to the PM, which supports surface expression of ORAI1. Although we did not check which cellular machinery is used for this fusion, it is likely that t-SNARE proteins syntaxin-4 and synaptosome associated protein 23 (SNAP-23), involved in vesicle fusion at the IS (Das et al., 2004), may play a role in this process. Another interesting question is the choreography of ORAI1 and STIM1 after the fusion of $ORAI1^+$ vesicles to the immunological synapse. It was shown that ORAI1 remains mobile in the PM and accumulates passively at the ER-PM junctions by a diffusion-trap mechanism, driven by its interaction with STIM1 (Prakriya and Lewis, 2015). Therefore, it is highly possible that STIM1 would influence surface insertion rate of ORAI1.

Embryonic development of *Drosophila melanogaster* requires *naked cuticle* (*nkd*) to attenuate a gradient of Wnt/β-catenin signaling. Nkd inhibits Wnt signaling by degrading Dvl. Mice and humans have two Nkd homologs, NKD1 and NKD2, that interact with Dvl, a homolog of *Drosophila* Dishevelled (Dsh), and inhibit Wnt signaling similar to their *Drosophila* homolog. However, mice deficient for both *Nkd1* and *Nkd2* showed normal embryonic development with subtle alterations in cranial bone structure (Zhang et al., 2007), pointing to their dispensable function during development in mammals. Interestingly, although NKD1 and NKD2 have a similar domain structure (e.g., EF-hands), their amino acid homology is just 43.8% (Katoh, 2001). In addition, while *NKD1* transcripts showed a broad expression pattern, *NKD2* mRNAs were expressed in selective tissues, including kidney, lung, and spleen (Katoh, 2001). Interestingly, our targeted screen did not identify NKD1 as a candidate for the regulation of CRAC channels, suggesting functional differences between the two homologs. Currently, we do not know whether *Drosophila* Nkd also acts as a regulator of *Drosophila* Orai, a homolog of the mammalian ORAI family.

Taken together, these studies suggest that NKD proteins evolved to have selective functions in mammals, as seen with NKD2 in the current study.

In conclusion, this study uncovered a novel mechanism that allows for high and sustained intracellular Ca^{2+} elevation via the CRAC channels in a leukemic cell line and primary T cells. We found that PM localization of ORAI1 channels is limited in effector T cells, with a significant fraction trapped in intracellular vesicles. After TCR stimulation, this intracellular pool trafficked to the PM to provide an additional source of ORAI1 channels. We have identified a key component of ORAI1 trafficking from a targeted screen as NKD2. The current work shows that NKD2 plays a specialized role in effector T cells by orchestrating $ORAI1^{+}$ vesicle trafficking in a TCR stimulation-dependent manner. *NKD2* gene, located on chromosome 5, has been linked to various T cell-related human diseases, including asthma, Crohn disease, and multiple sclerosis based on genome-wide association studies (Ahola-Olli et al., 2017; Baranzini et al., 2010; Franke et al., 2010; Hindorff et al., 2009; Moffatt et al., 2010). Understanding its role in T cells may reveal the impact of *NKD2* variations on human diseases and provide potential therapeutic targets for suppressing effector T cell-mediated autoimmune diseases.

STAR★METHODS

RESOURCE AVAILABILITY

Lead contact—Further information and requests for resources and reagents should be directed to and will be fulfilled by the Lead Contact, Sonal Srikanth (ssrikanth@mednet.ucla.edu).

Materials availability—All unique plasmids and/or cell lines generated in the study are available from the Lead Contact with a completed Materials Transfer Agreement.

Data and code availability

- This study did not generate any unique datasets.
- This paper does not report original code.
- Any additional information required to reanalyze the data reported in this paper is available from the lead contact upon request.

EXPERIMENTAL MODEL AND SUBJECT DETAILS

Cell lines and cultures—HEK293T, Jurkat E6-1 T cells, and Raji B cells were grown in complete DMEM (Mediatech) supplemented with 10% (v/v) fetal bovine serum (Hyclone), 2 mM L-glutamine (Mediatech), 10 mM HEPES (Mediatech) and Penicillin/Streptomycin (Mediatech) at 37°C and 5% CO2. Jurkat T cells were cultured in RPMI (Mediatech) containing 10% fetal bovine serum (Hyclone).

Human peripheral blood mononuclear cell culture—Peripheral blood mononuclear cells (PBMCs) were obtained under federal and state regulations from the CFAR Virology core Laboratory at UCLA that were prepared from buffy coats from healthy, unidentified

adult donors using Ficoll-PAQUE gradients. Naive CD4+ T cells were enriched by magnetic sorting from single-cell suspensions using MagniSort naive CD4+ T cell enrichment kit according to manufacturer's instructions (ThermoFisher Scientific). For effector T cell differentiation, cells were stimulated for 48 hours with plate-coated anti-CD3 antibody (10 μg/ml - OKT3, Bio X Cell) in the presence of soluble anti-CD28 antibody (5 μmg/ml, Bio X cell) in T cell media (DMEM containing 20% fetal bovine serum and 1% Pen-Strep) supplemented with 20 U/ml IL-2 (Peprotech) for T cell differentiation under non-polarizing conditions.

METHOD DETAILS

Plasmids—For the generation of cDNA library encoding the EF hand-containing candidates, cDNAs from HEK293T, HeLa or Jurkat T cells were used for PCR amplification and cloning of the candidates into pMSCV-CITE-eGFP-PGK-Puro vector with a C-terminal FLAG tag and expressing GFP from an IRES site (MO70). Transcript IDs of the candidates and primer sequences used for amplifying the candidates are indicated in Table S1. Various mutants of NKD2 were generated by PCR amplification and site-directed mutagenesis using primers described in Table S2. The EF-hand mutation of NKD2 replaced amino acids ^{132}DFD^{134} of NKD2 to AFA (NKD2$^{132DFD134 > AFA}$). cDNA encoding C-terminally FLAG-tagged NKD2 was subcloned into a lentiviral vector, FGllF (a kind gift from Dr. Dong Sun An, UCLA). The cDNAs encoding WT and mutants of NKD2 were also subcloned into pN1-mCherry and pEGFP-N1 vectors (Clontech) to generate C-terminally mCherry or GFP-fused proteins, respectively. For the construct of GFP-ORAI1-EC-HA plasmid based on the pMSCV-CITE-eGFP-PGK-Puro vector, GFP was fused at the N terminus of ORAI1 and an HA tag was inserted in the second extracellular loop between TM3 and TM4 of ORAI1 as previously described (Gwack et al., 2007). The ORAI1^{N223A}-TEV-pHluorin expression construct was designed to introduce the TEV target site flanked by spacer arms (amino acid sequence GSGSENLYFQGGAGA, TEV recognition sequence underlined) to both the N and C terminus of pHluorin (amplified from pCMV-lyso-pHluorin, Addgene) by PCR (Wienisch and Klingauf, 2006) followed by inserting it into the second extracellular loop between TM3 and TM4 of ORAI^{N223A}, to generate, ORAI1^{N223A}-EC-TEV-pHLuorin-TEV construct. ORAI1^{N223A} mutant of ORAI1 is not glycosylated in its extracellular loop region and shown to function simila to WT ORAI1 (Gwack et al., 2007), which is expected to provide better accessibility to the TEV protease.

Generation of NKD2 KO Jurkat T cells using the CRISPR-Cas9 system—To generate lentiviruses for transduction, HEK293T cells were transfected with plasmid(s) encoding sgRNA and packaging vectors (pMD2.G and psPAX2, Addgene) using calcium phosphate transfection method. Cas9-encoding lentivirus was generated using the same technique. Culture supernatants were harvested at 48- and 72-hours post-transfection and used for infection (50% of cas9-encoding virus + 50% of sgRNA-encoding virus) of Jurkat T cells with polybrene (8 μg/ml) using the spin-infection method. Cells were selected with puromycin (1 μg/ml) and blasticidin (5 μg/ml) 48 hours post-infection. The sgRNA sequences are described in Table S2.

Single-cell Ca^{2+} imaging, epifluorescence, TIRF, and confocal microscopy— Jurkat or primary T Cells were loaded at 1×10^6 cells/ml with 1 μM Fura 2-AM for 40 minutes at 25°C and attached to poly-L-lysine–coated coverslips. Intracellular $[Ca^{2+}]_i$ measurements were performed using essentially the same methods as previously described (Srikanth et al., 2010b). For Epifluorescence microscopy, HEK293T cells plated on cover glass-bottom dishes were stained with anti-FLAG antibodies or Jurkat T cells expressing indicated constructs were attached on poly-D-Lysine-coated dishes, visualized using 40X oil immersion lens and imaged using Slidebook software (Intelligent Imaging Innovations, Inc.). For TIRF analysis, coverslip bottom dishes were coated with 10 μg/ml of anti-CD3 antibody (OKT3) at 37°C for 1 hour, washed with PBS, and used for experiments. Cells were resuspended in Ringer's solution containing (mM): 155 NaCl, 4.5 KCl, 2 $CaCl_2$, 1 $MgCl_2$, 10 D-glucose, and 5 Na-HEPES (pH 7.4) and dropped onto anti-CD3 antibody-coated coverslips and used either for time-course imaging or fixed after stimulation for 10 mins with 2.5% PFA at room temperature and used for confocal analysis. TIRF microscopy was performed using an Olympus IX2 illumination system mounted on an Olympus IX51 inverted microscope using previously described methods (Srikanth et al., 2010a). Acquisition and image analysis were performed using Slidebook, and graphs were plotted using OriginPro (Originlab). For quantification of TIRF intensity across different cells, individual regions of interest were selected, and data were analyzed as the ratio of fluorescence intensity at each time-point (F) to that at the start of the experiment (F_0). Vesicle number quantification was performed using automated counting options in ImageJ. For confocal analysis, eGFP and mCherry were excited sequentially at 488 and 594 nm on a Fluoview FV10i Confocal Microscope (Olympus) with a 60x oil objective. Images were processed for enhancement of brightness or contrast using Fluoview software.

Immunoprecipitation and immunoblotting—For immunoprecipitation, cDNAs encoding 6xHis-tagged NKD2 and FLAG-tagged ORAI1 were transfected into HEK293T cells. Transfected cells (2×10^7) were lysed in cell lysis buffer (20 mM Tris-Cl, 2 mM EDTA, 135 mM NaCl, 10% (vol/vol) glycerol, 0.5% Igepal CA-630, and protease inhibitor mixture) and centrifuged at 100,000 x g for 1 hour before preclearing with protein G-Sepharose. Lysates were immunoprecipitated with anti-FLAG antibody-conjugated resin for 6 hours. Immunoprecipitates were washed five times in cell lysis buffer and analyzed by immunoblotting. For immunoblot analyses cells were lysed in RIPA buffer (10 mM Tris-Cl pH 8.0, 1% Triton X-100, 0.1% SDS, 140 mM NaCl, 1 mM EDTA, 0.1% sodium deoxycholate and protease inhibitor cocktail [Roche]) and centrifuged to remove debris. Samples were separated on 8%–10% SDS-PAGE. Proteins were transferred to nitrocellulose membranes and subsequently analyzed by immunoblotting with relevant antibodies. Chemiluminescence images were acquired using an Image reader LAS-3000 LCD camera (FujiFilm). For NKD2 dimerization with PKC-θ, HEK293T stably expressing 6xHis-tagged NKD2 together with empty vector or FLAG-tagged WT NKD2 or FLAG-tagged $NKD2^{S31A}$ in the presence or absence of PKC-θ were lysed in cell lysis buffer (same as above), precleared, and incubated with anti-FLAG antibody-conjugated resin overnight in cell lysis buffer containing 0.1% Igepal CA-630, and processed as described above. For nuclear NFAT analysis, Jurkat T cells were washed with ice-cold PBS and resuspended in prechilled cytoplasmic extraction buffer (20 mM Tris 7.5, 2 mM EDTA, 10 mM NaCl, 10%

glycerol, 0.1% Igepal CA-630) at the indicated time-points after ionomycin stimulation. Cells were centrifuged at 400 x g for 10 minutes. The supernatant was recovered as the cytoplasmic fraction and pellet was resuspended in nuclear extraction buffer (20 mM Tris 7.5, 2 mM EDTA, 500 mM NaCl, 10% glycerol, 1% Igepal CA-630). The extracts were centrifuged, and the supernatant was collected as a nuclear fraction. Both cytoplasmic and nuclear fractions were mixed with SDS loading dye and analyzed by immunoblotting.

Purification of recombinant proteins from *E. coli*—Fragments (aa 1-112, 113-178, 300-385, and 386-451) of NKD2 were subcloned into pGEX4T-1 plasmid using primers described in Table S2. GST fusion protein expressing transformants were grown in liquid cultures and induced with isopropyl-1-thio-β-D-galactopyranoside (IPTG, 0.2 mM) at 18°C overnight. Subsequently, cells were harvested and resuspended in lysis buffer (50 mM NaH_2PO_4, 500 mM NaCl, 10% glycerol, pH 8.0) containing protease inhibitors and 0.5% Triton X-100. Lysates were sonicated, centrifuged to remove debris and incubated with glutathione Sepharose 4B beads for 2 hr. After washing 8 times with lysis buffer, the beads were stored in lysis buffer without Triton X-100 at −20°C.

GST pulldown analysis—A vector encoding cDNA of full-length FLAG-ORAI1 was transfected into HEK293T cells. Transfected cells (2×10^7) were lysed in lysis buffer (20 mM Tris-Cl, 2 mM EDTA, 135 mM NaCl, 10% (vol/vol) glycerol, 0.5% Igepal CA-630, protease inhibitor mixture) and centrifuged at 100,000 x g for 1 hour before preclearing with protein G-Sepharose. Lysates were incubated with 20 μg of GST or GST-tagged NKD2 fragments of phospholipid binding domain (aa 1-112), Ca^{2+}-sensing EF-hand domain (EFh, aa 113-178), proline-rich domain (PRD, aa 300-385), and histidine-rich domain (aa 386-451) for 18 hours in binding buffer (1.0% Igepal CA-630, 20 mM Tris-HCl, 100 mM NaCl, 2 mM EDTA, protease inhibitors, 10% glycerol). Pulldown samples were washed five times with lysis buffer and analyzed by immunoblotting for indicated proteins.

Transfection, staining, and analysis of GFP-ORAI1-EC-HA construct—Exponentially growing control and NKD2 KO Jurkat T cells (3×10^6) were transfected with empty vector (pEGFPC1) or plasmids encoding GFP-ORAI1-EC-HA with or without wild-type or mutant NKD2 proteins by electroporation with an ECM 830 electroporator. Twenty-four hours after transfection, the cells were left untreated or stimulated with soluble anti-CD3 antibody (10 μg/ml, OKT3) and cross-linked with anti-mouse secondary antibody for indicated times. Cells were treated with anti-HA and secondary antibodies in PBS with 2% FBS on ice, subsequently, fixed with 4% paraformaldehyde (PFA) for 15 minutes at room temperature and analyzed with a FACSCalibur flow cytometer and FlowJo software. Naive $CD4^+$ T cells isolated from control and *Nkd2*$^{-/-}$ animals were transduced with retroviruses encoding empty vector or plasmids encoding ORAI1-EC-HA, cultured under non-polarizing for four days, and processed as described above.

TEV protease treatment of Jurkat T cells expressing ORAI1-EC-pHluorin—Control and NKD2 KO Jurkat T cells (3×10^6) were transfected with a plasmid encoding $ORAI1^{N223A}$-TEV-pHluorin by electroporation with an ECM 830 electroporator. Twenty-four hours after transfection, cells were left untreated or were stimulated with soluble

anti-CD3 antibody (10 μg/ml, OKT3) and cross-linked with anti-mouse secondary antibody for 20 minutes. Proteolytic cleavage was performed at room temperature (25°C) by adding 40 U TEV protease (Thermofisher) and 1 mM dithiothreitol (Thermofisher) for 20 min. The progress of cleavage was assayed by the loss of fluorescence using microscopy or flow cytometry.

Endogenous ORAI1 staining and analysis—For total endogenous ORAI1 detection, control, NKD2 KO cells, and ORAI1 KO cells (0.5×10^6) were fixed with 4% PFA at room temperature for 15 mins, followed by permeabilization with PBS + 0.5% Igepal CA-630 and incubated with 10 μg/ml unlabeled anti-ORAI1 antibody in PBS + 2% FBS + 0.5% Igepal CA-630. Cells were subsequently treated with secondary antibody, data was acquired on a BD Fortessa flow cytometer (BD Biosciences) and analyzed using FlowJo software. To mask all PM-resident ORAI1 and detect newly integrated endogenous surface ORAI1, control and NKD2 KO cells (0.5×10^6) were incubated with saturating amounts (10 μg/ml) of FITC-conjugated anti-ORAI1 EC antibody and subsequently stimulated with anti-CD3 antibody (10 μg/ml, OKT3) for indicated times and stained for newly integrated endogenous surface ORAI1 levels without permeabilization of cells using 5 μg/ml unlabeled anti-ORAI1 EC antibody. Cells were then treated with APC-conjugated secondary antibodies in PBS with 2% FBS on ice, subsequently, fixed with 4% PFA for 15 minutes at room temperature and analyzed with a FACSCalibur flow cytometer and FlowJo software.

Human peripheral blood mononuclear cell analysis—PBMCs were obtained under federal and state regulations from the CFAR Virology core Laboratory at UCLA that were prepared from buffy coats from healthy, unidentified adult donors using Ficoll-PAQUE gradients. Naive CD4+ T cells were enriched by magnetic sorting from single-cell suspensions using MagniSort naive CD4+ T cell enrichment kit according to manufacturer's instructions (ThermoFisher Scientific). For effector T cell differentiation, cells were stimulated for 48 hours with plate-coated anti-CD3 antibody (10 μg/ml - OKT3, Bio X Cell) in the presence of soluble anti-CD28 antibody (5 μg/ml, Bio X cell) in T cell media (DMEM containing 20% fetal bovine serum and 1% Pen-Strep) supplemented with 20 U/ml IL-2 (Peprotech) for T cell differentiation under non-polarizing conditions. For deletion of NKD2, cells were co-infected with lentiviruses encoding Cas9 and NKD2-targeting sgRNA#1 and sgRNA#3 on days 1 and 2 using the spin-infection method. On day 3, cells were selected with 1 μg/ml of puromycin and 5 μg/ml blasticidin for 2 days and then expanded for further 1 day with fresh media. On day 6, for cytokine staining, cells were re-stimulated with anti-CD3/anti-CD28 antibodies together with BrefeldinA (3 μg/ml) for 5 hours, fixed with 4% PFA for 15 minutes, permeabilized with 0.5% saponin, and stained with anti-IFN-γAb-PE, anti-IL-2 Ab-PE and anti-TNF Ab-APC. For T-bet staining, cells were fixed and permeabilized using Transcription Factor Staining Buffer Set and stained with APC-conjugated anti-T-bet antibody. For CTV Labeling experiment, PBMCs were labeled using CellTrace Violet Cell Proliferation Kit according to the manufacturer's protocols. CTV-labeled PBMCs were stimulated and transduced with lentiviruses for deletion of NKD2 as described above. The CTV-labeled cells were harvested and analyzed by flow cytometry on day 6.

QUANTIFICATION AND STATISTICAL ANALYSIS

Statistical significance was calculated using OriginPro and p values less than or equal to 0.05 were considered to be significant (*$p < 0.05$, **$p < 0.005$, ***$p < 0.0001$). For datasets with two groups, statistical analysis was performed with two-tailed t test to compare between control and test conditions. N numbers are described in each figure legends and data is represented as mean ± SEM.

Supplementary Material

Refer to Web version on PubMed Central for supplementary material.

ACKNOWLEDGMENTS

The authors thank Drs. No Hee Park, Ki Hyuk Shin, Mo K. Kang, and Reuben Kim (UCLA)for sharing their confocal imaging facility. Flow cytometry was performed in the UCLA Jonsson Comprehensive Cancer Center (JCCC) and Center for AIDS Research Flow Cytometry Core Facility that is supported by National Institutes of Health awards P30 CA016042 and 5P30 AI028697 and by the JCCC, the UCLA AIDS Institute, the David Geffen School of Medicine at UCLA, the UCLA Chancellor's Office, and the UCLA Vice Chancellor's Office of Research. This work was supported by the National Institute of Health grants AI083432, AI146615, AI147063, and AI149236 (Y.G.) and AI130653 and AI146352 (S.S.).

REFERENCES

Ahola-Olli AV, Würtz P, Havulinna AS, Aalto K, Pitkänen N, Lehtimäki T, Kähönen M, Lyytikäinen LP, Raitoharju E, Seppälä I, et al. (2017). Genome-wide Association Study Identifies 27 Loci influencing Concentrations of Circulating Cytokines and Growth Factors. Am. J. Hum. Genet 100, 40–50. [PubMed: 27989323]

Alderton JM, Ahmed SA, Smith LA, and Steinhardt RA (2000). Evidence for a vesicle-mediated maintenance of store-operated calcium channels in a human embryonic kidney cell line. Cell Calcium 28, 161–169. [PubMed: 11020378]

Altman A, Kaminski S, Busuttil V, Droin N, Hu J, Tadevosyan Y, Hipskind RA, and Villalba M (2004). Positive feedback regulation of PLCgamma1/Ca(2+) signaling by PKCtheta in restimulated T cells via a Tec kinase-dependent pathway. Eur. J. Immunol 34, 2001–2011. [PubMed: 15214048]

Baranzini SE, Srinivasan R, Khankhanian P, Okuda DT, Nelson SJ, Matthews PM, Hauser SL, Oksenberg JR, and Pelletier D (2010). Genetic variation influences glutamate concentrations in brains of patients with multiple sclerosis. Brain 133, 2603–2611. [PubMed: 20802204]

Barr VA, Bernot KM, Srikanth S, Gwack Y, Balagopalan L, Regan CK, Helman DJ, Sommers CL, Oh-Hora M, Rao A, and Samelson LE (2008). Dynamic movement of the calcium sensor STIM1 and the calcium channel Orai1 in activated T-cells: puncta and distal caps. Mol. Biol. Cell 19, 2802–2817. [PubMed: 18448669]

Choudhuri K, Llodrá J, Roth EW, Tsai J, Gordo S, Wucherpfennig KW, Kam LC, Stokes DL, and Dustin ML (2014). Polarized release of T-cell-receptor-enriched microvesicles at the immunological synapse. Nature 507, 118–123. [PubMed: 24487619]

Coudronniere N, Villalba M, Englund N, and Altman A (2000). NF-kappa B activation induced by T cell receptor/CD28 costimulation is mediated by protein kinase C-theta. Proc. Natl. Acad. Sci. USA 97, 3394–3399. [PubMed: 10716728]

Das V, Nal B, Dujeancourt A, Thoulouze MI, Galli T, Roux P, Dautry-Varsat A, and Alcover A (2004). Activation-induced polarized recycling targets T cell antigen receptors to the immunological synapse; involvement of SNARE complexes. Immunity 20, 577–588. [PubMed: 15142526]

Dong Y, Cao B, Zhang M, Han W, Herman JG, Fuks F, Zhao Y, and Guo M (2015). Epigenetic silencing of NKD2, a major component of Wnt signaling, promotes breast cancer growth. Oncotarget 6, 22126–22138. [PubMed: 26124080]

Esensten JH, Helou YA, Chopra G, Weiss A, and Bluestone JA (2016). CD28 Costimulation: From Mechanism to Therapy. Immunity 44, 973–988. [PubMed: 27192564]

Fasolato C, Hoth M, and Penner R (1993). A GTP-dependent step in the activation mechanism of capacitative calcium influx. J. Biol. Chem 268, 20737–20740. [PubMed: 8407897]

Feske S, Wulff H, and Skolnik EY (2015). Ion channels in innate and adaptive immunity. Annu. Rev. Immunol 33, 291–353. [PubMed: 25861976]

Franke A, McGovern DP, Barrett JC, Wang K, Radford-Smith GL, Ahmad T, Lees CW, Balschun T, Lee J, Roberts R, et al. (2010). Genomewide meta-analysis increasesto 71 the numberofconfirmed Crohn's disease susceptibility loci. Nat. Genet 42, 1118–1125. [PubMed: 21102463]

Gregory RB, and Barritt GJ (1996). Store-activated Ca2+ inflow in Xenopus laevis oocytes: inhibition by primaquine and evaluation of the role of membrane fusion. Biochem. J 319, 755–760. [PubMed: 8920977]

Gwack Y, Sharma S, Nardone J, Tanasa B, Iuga A, Srikanth S, Okamura H, Bolton D, Feske S, Hogan PG, and Rao A (2006). A genomewide Drosophila RNAi screen identifies DYRK-family kinases as regulators of NFAT. Nature 441, 646–650. [PubMed: 16511445]

Gwack Y, Srikanth S, Feske S, Cruz-Guilloty F, Oh-hora M, Neems DS, Hogan PG, and Rao A (2007). Biochemical and functional characterization of Orai proteins. J. Biol. Chem 282, 16232–16243. [PubMed: 17293345]

Hindorff LA, Sethupathy P, Junkins HA, Ramos EM, Mehta JP, Collins FS, and Manolio TA (2009). Potential etiologic and functional implications of genome-wide association loci for human diseases and traits. Proc. Natl. Acad. Sci. USA 106, 9362–9367. [PubMed: 19474294]

Hodeify R, Selvaraj S, Wen J, Arredouani A, Hubrack S, Dib M, Al-Thani SN, McGraw T, and Machaca K (2015). A STIM1-dependent 'trafficking trap' mechanism regulates Orai1 plasma membrane residence and Ca^{2+} influx levels. J. Cell Sci 128, 3143–3154. [PubMed: 26116575]

Hogan PG, Chen L, Nardone J, and Rao A (2003). Transcriptional regulation by calcium, calcineurin, and NFAT. Genes Dev. 17, 2205–2232. [PubMed: 12975316]

Irvine RF (1990). 'Quantal' Ca2+ release and the control of Ca2+ entry by inositol phosphates–a possible mechanism. FEBS Lett. 263, 5–9. [PubMed: 2185036]

Katoh M (2001). Molecular cloning, gene structure, and expression analyses of NKD1 and NKD2. Int. J. Oncol 19, 963–969. [PubMed: 11604995]

Kim KD, Srikanth S, Yee MK, Mock DC, Lawson GW, and Gwack Y (2011). ORAI1 deficiency impairs activated T cell death and enhances T cell survival. J. Immunol 187, 3620–3630. [PubMed: 21873530]

Kim KD, Srikanth S, Tan YV, Yee MK, Jew M, Damoiseaux R, Jung ME, Shimizu S, An DS, Ribalet B, et al. (2014). Calcium signaling via Orai1 is essential for induction ofthe nuclear orphan receptor pathway to drive Th17 differentiation. J. Immunol 192, 110–122. [PubMed: 24307733]

Kwon MJ, Ma J, Ding Y, Wang R, and Sun Z (2012). Protein kinase C-θ promotes Th17 differentiation via upregulation of Stat3. J. Immunol 188, 5887–5897. [PubMed: 22586032]

Lewis RS (2011). Store-operated calcium channels: new perspectives on mechanism and function. Cold Spring Harb. Perspect. Biol 3, a003970. [PubMed: 21791698]

Li C, Franklin JL, Graves-Deal R, Jerome WG, Cao Z, and Coffey RJ (2004). Myristoylated Naked2 escorts transforming growth factor alpha to the basolateral plasma membrane of polarized epithelial cells. Proc. Natl. Acad. Sci. USA 101, 5571–5576. [PubMed: 15064403]

Li C, Hao M, Cao Z, Ding W, Graves-Deal R, Hu J, Piston DW, and Coffey RJ (2007). Naked2 acts as a cargo recognition and targeting protein to ensure proper delivery and fusion of TGF-alpha containing exocytic vesicles at the lower lateral membrane of polarized MDCK cells. Mol. Biol. Cell 18, 3081–3093. [PubMed: 17553928]

Lin X, O'Mahony A, Mu Y, Geleziunas R, and Greene WC (2000). Protein kinase C-theta participates in NF-kappaB activation induced by CD3-CD28 costimulation through selective activation of IkappaB kinase beta. Mol. Cell. Biol 20, 2933–2940. [PubMed: 10733597]

Lioudyno MI, Kozak JA, Penna A, Safrina O, Zhang SL, Sen D, Roos J, Stauderman KA, and Cahalan MD (2008). Orai1 and STIM1 move to the immunological synapse and are up-regulated during T cell activation. Proc. Natl. Acad. Sci. USA 105, 2011–2016. [PubMed: 18250319]

Ma J, Ding Y, Fang X, Wang R, and Sun Z (2012). Protein kinase C-θ inhibits inducible regulatory T cell differentiation via an AKT-Foxo1/3a-dependent pathway. J. Immunol 188, 5337–5347. [PubMed: 22539794]

Miesenböck G, De Angelis DA, and Rothman JE (1998). Visualizing secretion and synaptic transmission with pH-sensitive green fluorescent proteins. Nature 394, 192–195. [PubMed: 9671304]

Moffatt MF, Gut IG, Demenais F, Strachan DP, Bouzigon E, Heath S, von Mutius E, Farrall M, Lathrop M, Cookson WOCM, et al. (2010). A large-scale, consortium-based genomewide association study of asthma. N. Engl. J. Med 363, 1211–1221. [PubMed: 20860503]

Parekh AB, and Penner R (1997). Store depletion and calcium influx. Physiol. Rev 77, 901–930. [PubMed: 9354808]

Parekh AB, and Putney JW Jr. (2005). Store-operated calcium channels. Physiol. Rev 85, 757–810. [PubMed: 15788710]

Pfeifhofer C, Kofler K, Gruber T, Tabrizi NG, Lutz C, Maly K, Leitges M, and Baier G (2003). Protein kinase C theta affects Ca2+ mobilization and NFAT cell activation in primary mouse T cells. J. Exp. Med 197, 1525–1535. [PubMed: 12782715]

Prakriya M, and Lewis RS (2015). Store-Operated Calcium Channels. Physiol. Rev 95, 1383–1436. [PubMed: 26400989]

Putney JW Jr., Broad LM, Braun FJ, Lievremont JP, and Bird GS (2001). Mechanisms of capacitative calcium entry. J. Cell Sci 114, 2223–2229. [PubMed: 11493662]

Quann EJ, Liu X, Altan-Bonnet G, and Huse M (2011). A cascade of protein kinase C isozymes promotes cytoskeletal polarization in T cells. Nat. Immunol 12, 647–654. [PubMed: 21602810]

Randriamampita C, and Tsien RY (1993). Emptying of intracellular Ca2+ stores releases a novel small messenger that stimulates Ca2+ influx. Nature 364, 809–814. [PubMed: 8355806]

Ritchie MF, Samakai E, and Soboloff J (2012). STIM1 is required for attenuation of PMCA-mediated Ca(2+) clearance during T-cell activation. EMBO J. 31, 1123–1133. [PubMed: 22246182]

Rousset R, Wharton KA Jr., Zimmermann G, and Scott MP (2002). Zinc-dependent interaction between dishevelled and the Drosophila Wnt antagonist naked cuticle. J. Biol. Chem 277, 49019–49026. [PubMed: 12354775]

Shi X, Bi Y, Yang W, Guo X, Jiang Y, Wan C, Li L, Bai Y, Guo J, Wang Y, et al. (2013). Ca2+ regulates T-cell receptor activation by modulating the charge property of lipids. Nature 493, 111–115. [PubMed: 23201688]

Soares H, Henriques R, Sachse M, Ventimiglia L, Alonso MA, Zimmer C, Thoulouze MI, and Alcover A (2013). Regulated vesicle fusion generates signaling nanoterritories that control T cell activation at the immunological synapse. J. Exp. Med 210, 2415–2433. [PubMed: 24101378]

Somasundaram B, Norman JC, and Mahaut-Smith MP (1995). Primaquine, an inhibitor of vesicular transport, blocks the calcium-release-activated current in rat megakaryocytes. Biochem. J 309, 725–729. [PubMed: 7639685]

Srikanth S, and Gwack Y (2013). Orai1-NFAT signalling pathway triggered by T cell receptor stimulation. Mol. Cells 35, 182–194. [PubMed: 23483280]

Srikanth S, Jung HJ, Kim KD, Souda P, Whitelegge J, and Gwack Y (2010a). A novel EF-hand protein, CRACR2A, is a cytosolic Ca2+ sensor that stabilizes CRAC channels in T cells. Nat. Cell Biol 12, 436–446. [PubMed: 20418871]

Srikanth S, Jung HJ, Ribalet B, and Gwack Y (2010b). The intracellular loop of Orai1 plays a central role in fast inactivation of Ca2+ release-activated Ca2+ channels. J. Biol. Chem 285, 5066–5075. [PubMed: 20007711]

Sun Z, Arendt CW, Ellmeier W, Schaeffer EM, Sunshine MJ, Gandhi L, Annes J, Petrzilka D, Kupfer A, Schwartzberg PL, and Littman DR (2000). PKC-theta is required for TCR-induced NF-kappaB activation in mature but not immature T lymphocytes. Nature 404, 402–407. [PubMed: 10746729]

Tan YX, Manz BN, Freedman TS, Zhang C, Shokat KM, and Weiss A (2014). Inhibition of the kinase Csk in thymocytes reveals a requirement for actin remodeling in the initiation of full TCR signaling. Nat. Immunol 15, 186–194. [PubMed: 24317039]

Wienisch M, and Klingauf J (2006). Vesicular proteins exocytosed and subsequently retrieved by compensatory endocytosis are nonidentical. Nat. Neurosci 9, 1019–1027. [PubMed: 16845386]

Woodard GE, Salido GM, and Rosado JA (2008). Enhanced exocytotic-like insertion of Orai1 into the plasma membrane upon intracellular Ca2+ store depletion. Am. J. Physiol. Cell Physiol 294, C1323–C1331. [PubMed: 18400989]

Yao Y, Ferrer-Montiel AV, Montal M, and Tsien RY (1999). Activation of store-operated Ca2+ current in Xenopus oocytes requires SNAP-25 but not a diffusible messenger. Cell 98, 475–485. [PubMed: 10481912]

Yu F, Sun L, and Machaca K (2009). Orai1 internalization and STIM1 clustering inhibition modulate SOCE inactivation during meiosis. Proc. Natl. Acad. Sci. USA 106, 17401–17406. [PubMed: 19805124]

Yu F, Sun L, and Machaca K (2010). Constitutive recycling of the store-operated Ca2+ channel Orai1 and its internalization during meiosis. J. Cell Biol 191, 523–535. [PubMed: 21041445]

Zanin-Zhorov A, Dustin ML, and Blazar BR (2011). PKC-θ function at the immunological synapse: prospects for therapeutic targeting. Trends Immunol. 32, 358–363. [PubMed: 21733754]

Zeng W, Wharton KA Jr., Mack JA, Wang K, Gadbaw M, Suyama K, Klein PS, and Scott MP (2000). naked cuticle encodes an inducible antagonist of Wnt signalling. Nature 403, 789–795. [PubMed: 10693810]

Zhang Q, and Vignali DA (2016). Co-stimulatory and Co-inhibitory Pathways in Autoimmunity. Immunity 44, 1034–1051. [PubMed: 27192568]

Zhang S, Cagatay T, Amanai M, Zhang M, Kline J, Castrillon DH, Ashfaq R, Oz OK, and Wharton KA Jr. (2007). Viable mice with compound mutations in the Wnt/Dvl pathway antagonists nkd1 and nkd2. Mol. Cell. Biol 27, 4454–4464. [PubMed: 17438140]

Zhao S, Kurenbekova L, Gao Y, Roos A, Creighton CJ, Rao P, Hicks J, Man TK, Lau C, Brown AM, et al. (2015). NKD2, a negative regulator of Wnt signaling, suppresses tumor growth and metastasis in osteosarcoma. Oncogene 34, 5069–5079. [PubMed: 25579177]

Highlights

- Sustained activation of the CRAC channel is pivotal for effector T cell responses
- Plasma membrane localization of ORAI1 is limited in effector T cells
- NKD2 is an adaptor molecule activated by signaling pathways downstream of TCRs
- NKD2 orchestrates trafficking of ORAI1^{+} vesicles to the plasma membrane

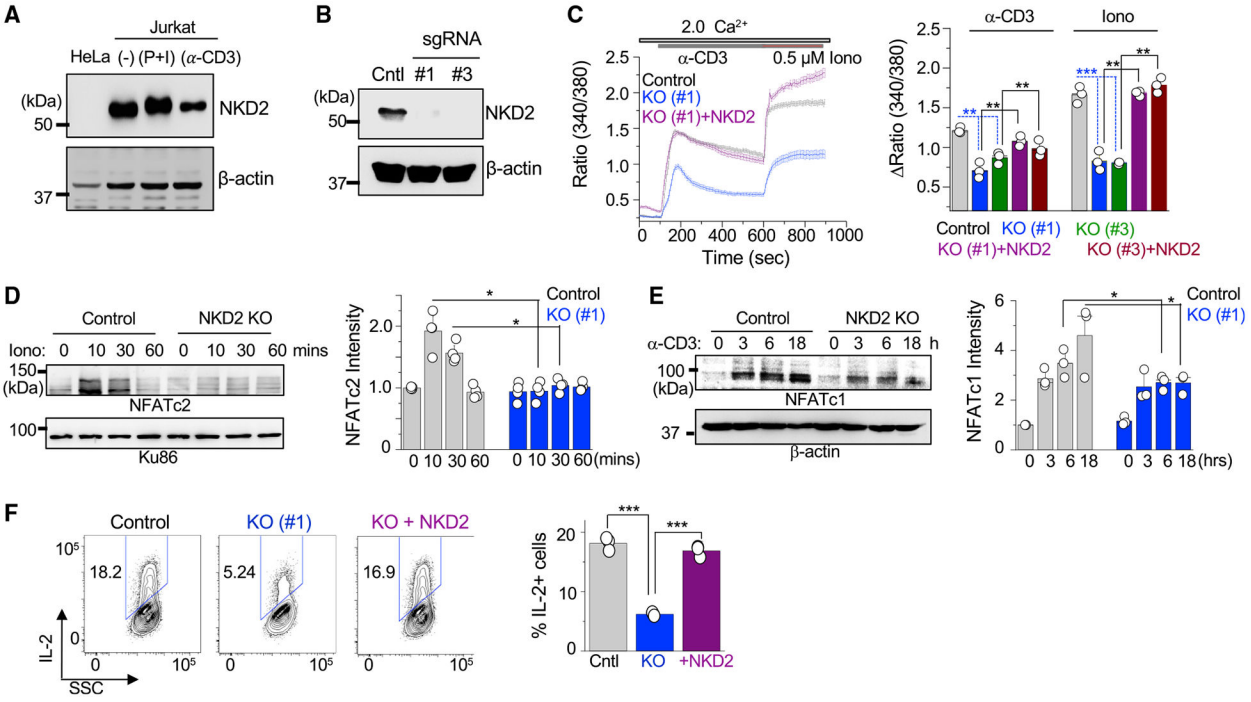

Figure 1. NKD2 is involved in regulation of the Ca^{2+}-NFAT signaling pathway in T cells

(A) Representative immunoblot showing expression of NKD2 in lysates from HeLa cells, unstimulated Jurkat T cells, or those stimulated with PMA + ionomycin or anti-CD3 antibody (Ab) for 6 h. β-Actin, loading control. Data are representative of two independent experiments.

(B) Representative immunoblot showing expression of NKD2 in lysates of control or NKD2 knockout (KO) Jurkat T cells generated using two independent sgRNAs (#1 and #3). β-Actin, loading control. Data are representative of two independent experiments.

(C) Representative traces showing averaged SOCE from control (69 cells), NKD2 KO (KO sgRNA #1, 70 cells) Jurkat T cells, or NKD2 KO Jurkat T cells reconstituted for expression of NKD2 (KO sgRNA #1 + NKD2, 68 cells) after TCR stimulation using anti-CD3 antibodies, followed by ionomycin treatment in the presence of external solution containing 2 mM Ca^{2+}. Bar graph (right) shows averaged baseline-subtracted SOCE (±SEM) from three independent experiments with NKD2 KO cells generated using two independent sgRNAs (#1 and #3).

(D) Representative immunoblot of NFATc2 levels in nuclear extracts from wild-type (WT) and NKD2 KO (sgRNA #1) Jurkat T cells stimulated with 1 μM ionomycin for indicated times. A nuclear protein, Ku86, was used as a loading control. Bar graph shows the densitometric analysis of relative band intensities of nuclear NFATc2. Data show means ± SEM of pooled technical replicates from two independent nuclear extracts.

(E) Representative immunoblot showing expression of NFATc1 in total cellular lysates from WT and NKD2 KO (sgRNA #1) Jurkat T cells stimulated with anti-CD3 and anti-CD28 antibodies for the indicated times. β-Actin, loading control. Bar graph shows the densitometric analysis of relative band intensities of total NFATc1. Data show means ± SEM of pooled technical replicates from two independent cellular lysates.

(F) Representative flow plots showing expression of IL-2 in control, NKD2 KO (sgRNA #1) Jurkat T cells, or NKD2 KO Jurkat T cells expressing NKD2 after stimulation with PMA + ionomycin for 16 h. Bar graph shows means ± SEM from three independent experiments. *$p < 0.05$; **$p < 0.005$; ***$p < 0.0001$.

See also Figures S1, S2, and Table S1.

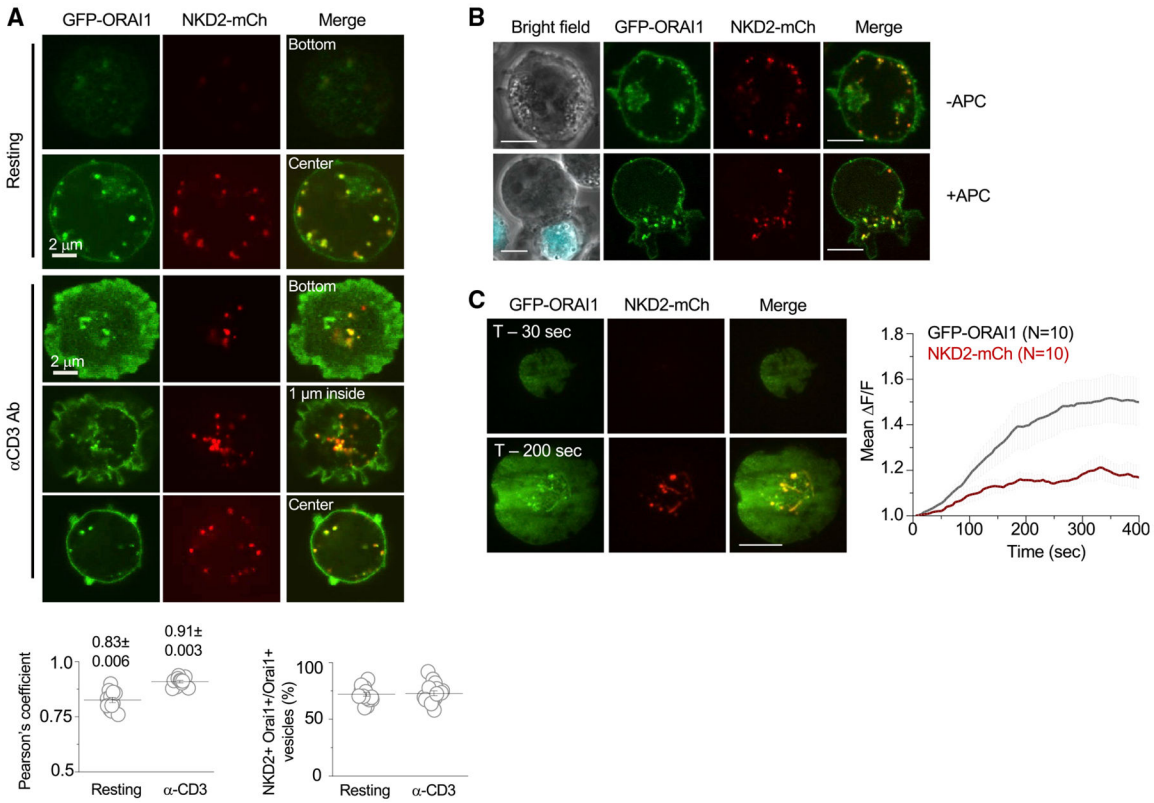

Figure 2. Localization of NKD2 in intracellular ORAI1$^+$ vesicles

(A) Top: representative confocal images of Jurkat T cells expressing GFP-ORAI1 and NKD2-mCherry (NKD2-mCh) under resting conditions (top two panels) or 10 min after dropping onto anti-CD3 Ab-coated coverslips. Images represent different depths within the cells, as indicated. Data are representative of similar observations from 10 (resting) and 16 (anti-CD3 Ab-stimulated) cells in two independent experiments. Bottom: scatterplot showing Pearson's correlation coefficient for colocalization between ORAI1 and NKD2 under resting (13 cells) or anti-CD3 Ab-stimulated (13 cells) conditions from two independent experiments (left). Scatterplot showing percentage of Orai1$^+$ NKD2$^+$ vesicles among the Orai1$^+$ vesicles under resting (16 cells) and anti-CD3 Ab-stimulated (16 cells) conditions from two independent experiments (right).

(B) Representative confocal images of Jurkat T cells expressing GFP-ORAI1 and NKD2-mCh under resting conditions (top panels) or 30 min after stimulation with staphylococcal enterotoxin E (SEE)-pulsed Raji B cells loaded with CellTracer Blue CMAC (7-amino-4-chloromethylcoumarin) dye. Leftmost panel shows bright-field images overlaid with Raji B cells in blue in the bottom panel. Data are representative of similar observations from 10 (resting) and 14 (stimulated) cells in two independent experiments. Scale bar, 5 μm.

(C) Representative TIRF images of a Jurkat T cell expressing GFP-ORAI1 and NKD2-mCh at early (30 s, top panels) and later (200 s, bottom panels) time points after dropping onto anti-CD3 Ab-coated coverslip. The line graph on the right shows normalized (mean ± SEM) fluorescence intensities from indicated cell numbers (N) depicting kinetics of accumulation of ORAI1 and NKD2 at the site of contact between the cell and the coverslip. Scale bar, 5 μm.

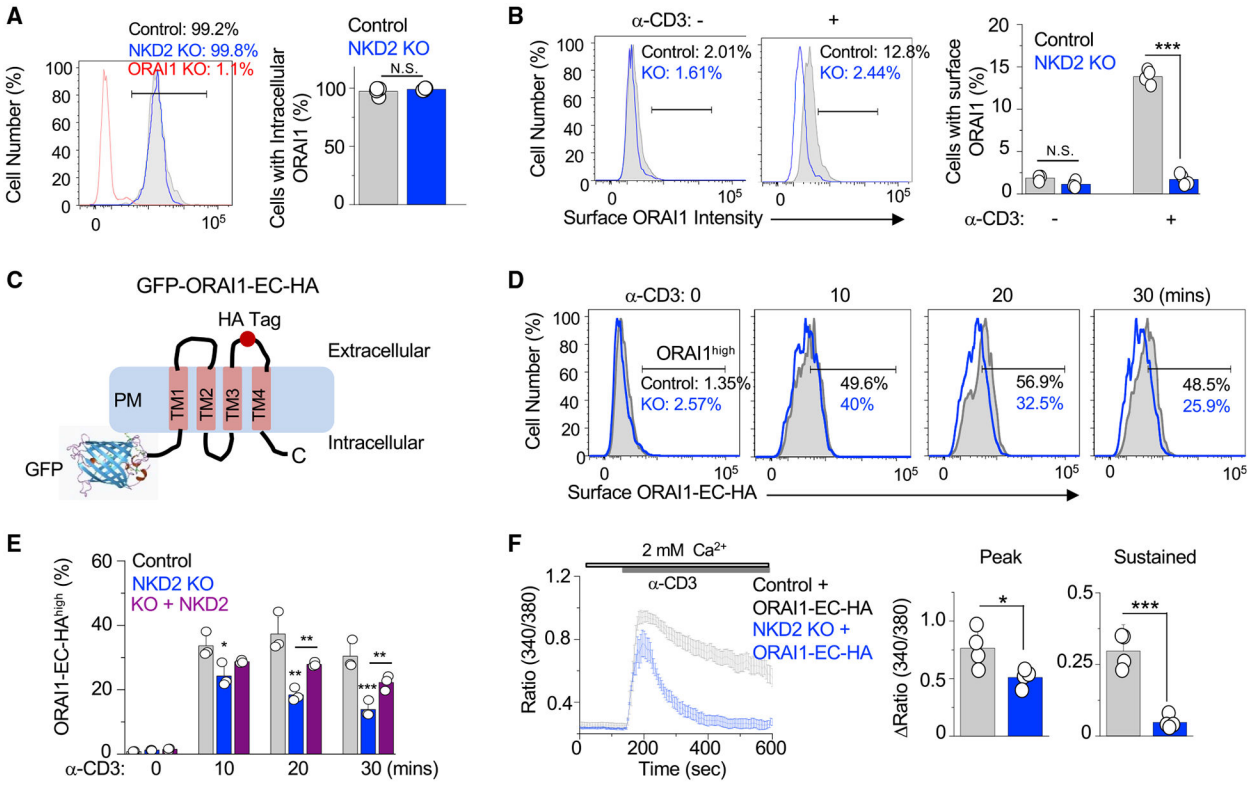

Figure 3. NKD2 is essential for stimulation-induced surface expression of ORAI1

(A) Representative histograms showing levels of total ORAI1 protein in control, NKD2 KO, and ORAI1 KO Jurkat T cells after permeabilization and intracellular staining with anti-ORAI1 Ab. The bar graph shows average (±SEM) from four independent experiments.

(B) Representative histograms showing levels of newly inserted PM-resident ORAI1 protein in control and NKD2 KO Jurkat T cells after TCR stimulation. Cells were incubated with saturating amounts of fluorescein isothiocyanate (FITC)-conjugated anti-ORAI1 Ab (to mask all PM-resident ORAI1) before stimulation with anti-CD3 Ab for 20 min. Subsequently, the cells were stained with unlabeled anti-ORAI1 Ab and APC-labeled secondary antibody without permeabilization to detect newly integrated surface ORAI1 protein. Bar graph shows average (±SEM) from four independent experiments.

(C) Schematic of GFP-ORAI1-EC-HA construct. GFP is fused to the N terminus of ORAI1, and an HA tag is inserted in the second extracellular loop between transmembrane segments TM3 and TM4 of ORAI1.

(D) Representative flow plots showing frequencies of ORAI1^{high} population in control and NKD2 KO Jurkat T cells expressing GFP-ORAI1-EC-HA at indicated time points after stimulation with anti-CD3 Ab. Non-permeabilized cells were stained with anti-HA Abs to label PM-localized ORAI1 as described in (B). Gating strategy is described in Figure S3.

(E) Bar graph showing surface expression of GFP-ORAI1-EC-HA in control, NKD2 KO Jurkat T cells, and NKD2 KO cells reconstituted for expression of NKD2 (KO + NKD2) after TCR stimulation (as demonstrated in D). Data show means ± SEM from three independent experiments.

(F) Representative traces showing averaged SOCE from control (20 cells) and NKD2 KO (KO sgRNA #1, 20 cells) Jurkat T cells expressing GFP-ORAI1-EC-HA after TCR stimulation using anti-CD3 Abs in the presence of external solution containing 2 mM Ca^{2+}. Bar graphs show averaged baseline-subtracted SOCE (±SEM) at the peak and later time point (600 s, sustained) from four independent experiments.
*$p < 0.05$; **$p < 0.005$; ***$p < 0.0001$.
See also Figure S3.

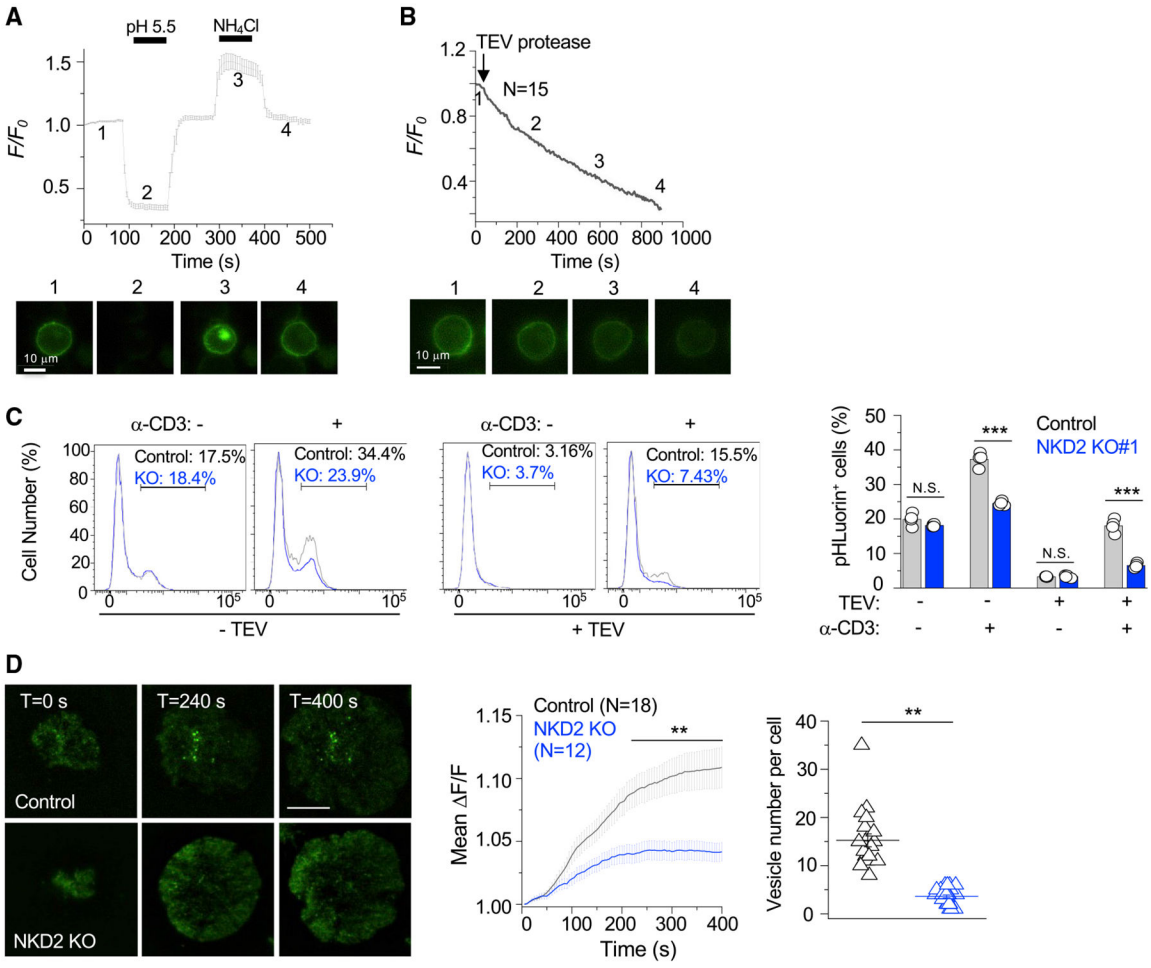

Figure 4. Visualization of ORAI1^{+} vesicle trafficking using a pH-sensitive biomarker

(A) Line graph showing the averaged (±SEM) kinetics of normalized fluorescence changes in 20 Jurkat cells expressing ORAI1-EC-pHluorin upon exposure to acidic solution (pH 5.5) or ammonium chloride (50 mM). Images below show the fluorescence intensity of a representative cell at the time points indicated by numbers in the graph above.

(B) Line graph showing the averaged (±SEM) kinetics of normalized fluorescence changes in 15 Jurkat T cells expressing ORAI1-EC-pHluorin after treatment with TEV protease at the indicated time points. Images below show the fluorescence intensity of a representative cell at the time points indicated by numbers in the graph above.

(C) Representative flow plots showing frequencies of pHluorin^{+} populations in control and NKD2 KO Jurkat T cells expressing ORAI1-EC-pHluorin under resting conditions or 20 min after stimulation with anti-CD3 and cross-linking Abs. Cells were untreated (−TEV) or treated with TEV protease (+TEV, 15 min) before stimulation. Bar graph shows means ± SEM of pooled technical replicates from three independent experiments.

(D) Representative TIRF images of control (top panels) and NKD2 KO (bottom panels) Jurkat T cells expressing ORAI1-EC-pHluorin at the indicated time points after dropping onto anti-CD3 Ab-coated coverslips. The line graph (middle) shows normalized (mean ± SEM) fluorescence intensities from indicated cell numbers (N) depicting the kinetics of

insertion of ORAI1^{+} vesicles on the PM. The scatter graph on the right depicts the number of vesicles inserted in control or NKD2 KO Jurkat T cell expressing ORAI1-EC-pHluorin. Each symbol represents data from an independent cell. Scale bar, 5 μm.
**p < 0.005; ***p < 0.0001.

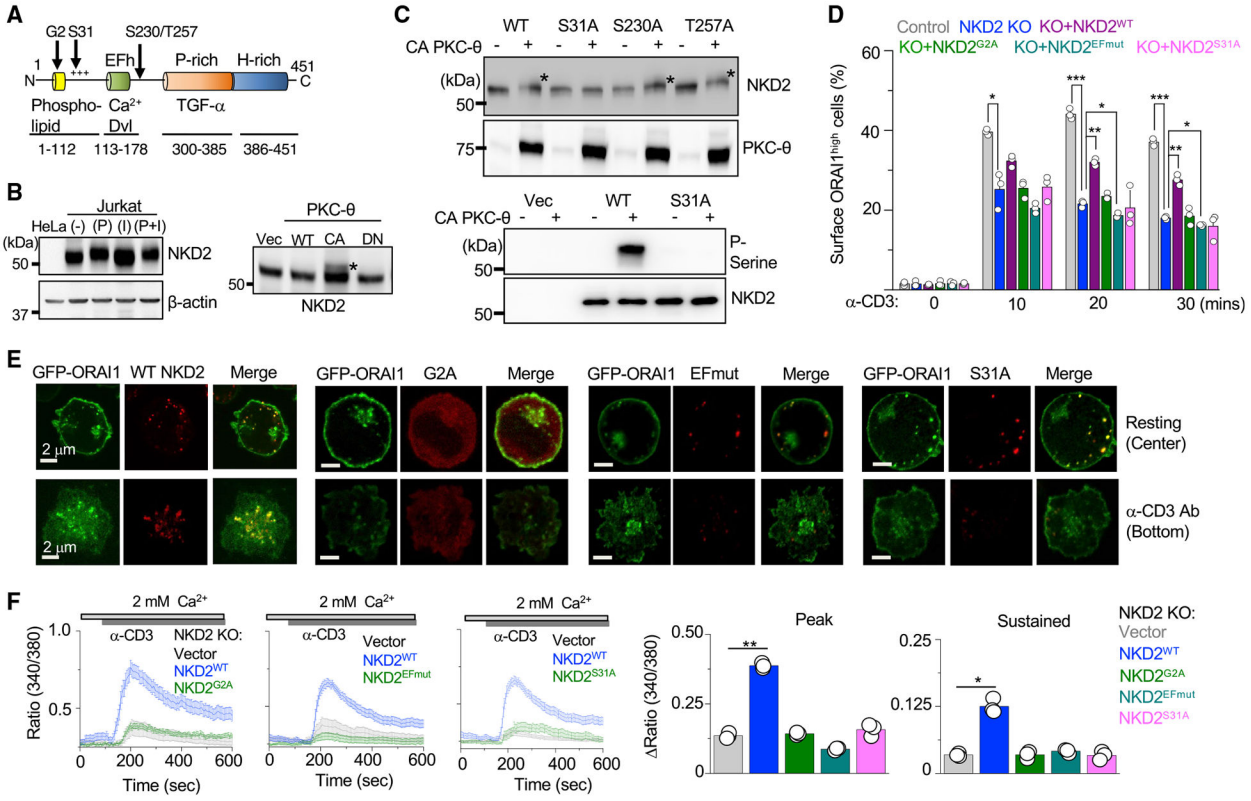

Figure 5. Ca^{2+} sensing, phosphorylation, and myristoylation are required for NKD2-mediated $ORAI1^{+}$ vesicle trafficking

(A) Schematic showing the domain structure of NKD2. NKD2 contains a myristoylation motif at the second glycine residue (G2), putative PKC phosphorylation sites (S31, S230, and T257), a Ca^{2+}-binding EF-hand (known to interact with Dishevelled), a TGF-α-binding proline-rich domain, and a histidine-rich C terminus.

(B) Left: representative immunoblot showing NKD2 expression in lysates from HeLa cells; unstimulated Jurkat T cells; or those stimulated with PMA, ionomycin, or PMA + ionomycin (left). β-Actin, loading control. Right: representative immunoblot for detection of NKD2 in lysates from HEK293T cells expressing NKD2 together with empty vector (Vec), WT PKC-θ, a constitutive active mutant of PKC-θ (CA), or a dominant-negative mutant of PKC-θ (DN) (right). Asterisk (*) indicates a band corresponding to phosphorylated NKD2. Data are representative of two independent experiments.

(C) Top: representative immunoblot showing the molecular weight shift of WT and indicated mutants of NKD2 in lysates of HEK293T cells co-expressing constitutive active PKC-θ (CA PKC-θ; top two panels). Asterisk (*) indicates a band corresponding to phosphorylated NKD2. Bottom: representative immunoblot for detection of phosphorylated NKD2. Lysates of HEK293T cells co-expressing WT or S31A mutant of FLAG-tagged NKD2 with CA PKC-θ were immunoprecipitated with FLAG resin and immunoblotted for detection of phosphorylated NKD2 using phospho-serine Abs. Bottom: NKD2 from FLAG immunoprecipitates as loading controls. Images are representative of two independent experiments.

(D) Frequencies of ORAI1^{high} population in control and NKD2 KO Jurkat T cells expressing GFP-ORAI1-EC-HA together with mCh-tagged WT or indicated mutants of NKD2. At the indicated time points after stimulation with anti-CD3 Abs, cells were stained with anti-HA antibodies without permeabilization to label PM-localized ORAI1. Data are average ± SEM from three independent experiments.

(E) Representative confocal images of Jurkat T cells expressing GFP-ORAI1 and NKD2^{WT}-mCh, NKD2^{G2A}-mCh (G2A), NKD2$^{132DFD>AFA}$-mCh (EFmut), and NKD2^{S31A}-mCh (S31A) under resting conditions (top panels) or 20 min after dropping on stimulatory anti-CD3 antibody-coated coverslips (bottom panels). The top panels show images from the center of the cell, whereas the bottom panels show images from the bottom of the cell, which is in contact with the coverslip. Images are representative of at least 10 cells in each condition. Scale bar, 2 μm.

(F) Representative traces showing averaged SOCE from NKD2 KO Jurkat T cells expressing empty vector (40 cells), NKD2^{WT}-mCh (35 cells), NKD2^{G2A}-mCh (30 cells), NKD2$^{132DFD>AFA}$-mCh (30 cells), or NKD2^{S31A}-mCh (30 cells) after TCR stimulation using anti-CD3 Abs in the presence of external solution containing 2 mM Ca^{2+}. Bar graphs (right) show averaged baseline-subtracted SOCE (±SEM) at the peak and later time point (600 s, sustained) from three independent experiments.

*$p < 0.05$; **$p < 0.005$; ***$p < 0.0001$.

See also Figures S4 and S5.

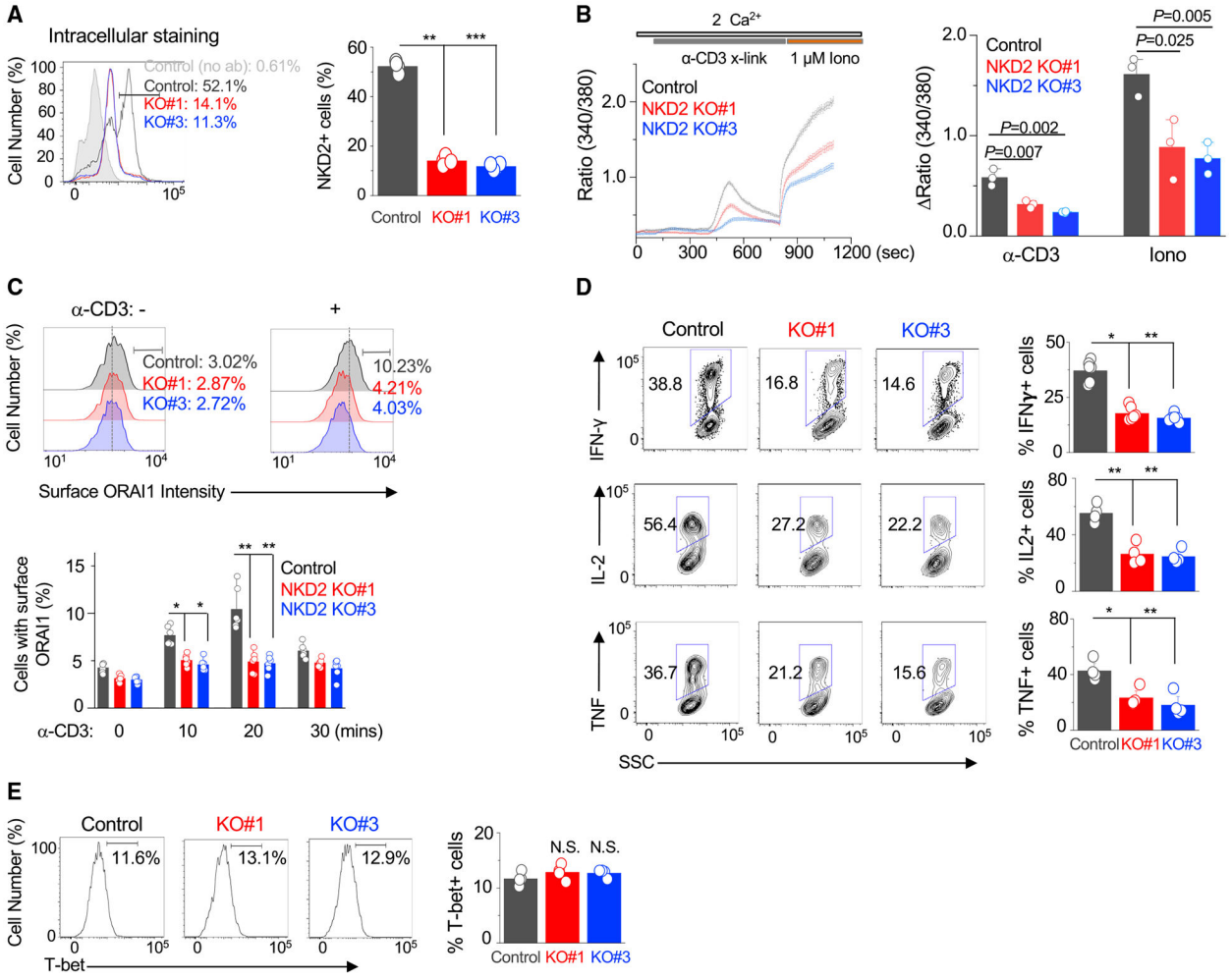

Figure 6. NKD2-mediated ORAI1^{+} vesicle trafficking is crucial for the effector function of primary T cells

(A) Representative histograms showing levels of NKD2 protein in primary T cells transduced with lentiviral vectors encoding scrambled sgRNA (control), NKD2 sgRNA #1, and NKD2 sgRNA #3, together with those encoding Cas9. Cells were permeabilized and stained with anti-NKD2 Ab. The bar graph (right) shows average (±SEM) from four independent experiments.

(B) Representative traces showing averaged SOCE from primary control (73 cells) and NKD2 KO (KO sgRNA #1, 82 cells; KO sgRNA #3, 71 cells) T cells after TCR stimulation using anti-CD3 Abs, followed by ionomycin treatment in the presence of external solution containing 2 mM Ca^{2+}. Bar graph (right) shows averaged baseline-subtracted SOCE (±SEM) from three independent experiments.

(C) Representative histograms showing levels of newly inserted PM-resident ORAI1 protein in primary control and *NKD2* KO effector T cells after TCR stimulation. Cells were transduced as described above to induce deletion of *NKD2* and stimulated and stained as described in Figure 3B for detection of newly inserted PM-resident ORAI1. Bar graph (right) shows average (±SEM) of pooled technical replicates from three independent donors.

(D) Representative flow plots showing expression of IFN-γ, IL-2, and TNF in control, NKD2 KO (sgRNA #1), and NKD2 KO (sgRNA #3) cells after re-stimulation with anti-CD3 and anti-CD28 Abs. Bar graph shows means ± SEM of pooled technical replicates from two independent experiments.
(E) Representative histograms showing levels of T-bet in control, NKD2 KO (sgRNA #1), and NKD2 KO (sgRNA #3) cells. Bar graph shows means ± SEM of pooled technical replicates from two independent experiments.
*$p < 0.05$; **$p < 0.005$; ***$p < 0.0001$.
See also Figure S6.

KEY RESOURCES TABLE

REAGENT or RESOURCE	SOURCE	IDENTIFIER
Antibodies		
Human NKD2	Cell Signaling Technologies	Cat# 2073
Phospho-Erk	Cell Signaling Technologies	Cat# 4377
Erk	Cell Signaling Technologies	Cat# 9102
Phospho-p38	Cell Signaling Technologies	Cat# 4511
p38	Cell Signaling Technologies	Cat# 9212
Phospho-JNK	Cell Signaling Technologies	Cat# 9255
JNK	Cell Signaling Technologies	Cat# 9252
PKCθ	Cell Signaling Technologies	Cat# 13643
STIM1	Cell Signaling Technologies	Cat# 5668S
STIM2	Cell Signaling Technologies	Cat# 4917
Phospho-IkB	Cell Signaling Technologies	Cat# 9246
β-Catenin	Cell Signaling Technologies	Cat# 9562
Phospho-mTOR	Cell Signaling Technologies	Cat# 2971
Phospho-p70 S6	Cell Signaling Technologies	Cat# 9205
His tag	Cell Signaling Technologies	Cat# 12698S
FLAG tag	Millipore Sigma	Cat# F3040
HA tag	Millipore Sigma	Cat# 15782900
Human ORAI1 (immunoblotting)	Millipore Sigma	Cat# AB9868
Human ORAI1 (flow cytometry)	Alomone Labs	Cat# ACC-060; ACC-060-F
β-actin	Santa Cruz Biotechnology	Cat# sc-47778
NFATc2	Santa Cruz Biotechnology	Cat# sc-7296
Ku-86	Santa Cruz Biotechnology	Cat# sc-5280
Phospho-Serine	Santa Cruz Biotechnology	Cat# sc-81514
PMCA4b	Santa Cruz Biotechnology	Cat# sc-20027
NFATc1	BD PharMingen	Cat# 556602
α-CD3 antibody	Bio X Cell	Cat# BE0001-2
α-CD28 antibody	Bio X Cell	Cat# BE0248
α-IFN-γ Ab-PE (clone 45.B3)	eBioscience	Cat# 12-7319-42
α-IL-2 Ab-PE (clone MQ1-17H12)	eBioscience	Cat# 12-7029-81
α-TNF Ab-APC (clone MAb11)	eBioscience	Cat# 17-7349-41
α-T-bet Ab-APC (clone 4B10)	eBioscience	Cat# 2124193
Bacterial and virus strains		
E. coli DH5α	Thermo fisher Scientific	Cat# 18265017
Chemicals, peptides, and recombinant proteins		
Fura 2-AM	Thermofisher Scientific	Cat# F1221
Brefeldin A	Thermofisher Scientific	Cat# 00-4506-51
Thapsigargin	EMD Millipore	Cat# 80055-474
Phorbol 12-myristate 13-acetate (PMA)	EMD Millipore	Cat# 5.00582.0001
Ionomycin	EMD Millipore	Cat# 407951

REAGENT or RESOURCE	SOURCE	IDENTIFIER
Polybrene	Millipore Sigma	Cat# TR-1003
Puromycin	Invivogen	Cat# ant-pr-1
Blasticidin	Invivogen	Cat# ant-bl-05
Poly-D-Lysine	Thermo Fisher Scientific	Cat# A003E
Glutathione Sepharose 4B beads	Thermo Fisher Scientific	Cat# 101041
TEV protease	Thermofisher	Cat# T4455
IL-2	Peprotech	Cat# 200-02
Fixable Viability Dye eFluor 780	eBioscience	Cat# 65-0865-14
Critical commercial assays		
MagniSort human naive CD4+ T cell enrichment kit	ThermoFisher Scientific	Cat# 8804-6814-74
CellTrance Violet Cell Proliferation kit	ThermoFisher Scientific	Cat# C34557
FOXP3/Transcription Factor staining Buffer set	ThermoFisher Scientific	Cat# 2229155
Experimental models: Cell lines		
HEK293T	ATCC	Cat# CRL-3216
Jurkat E6-1 T cells	ATCC	Cat# TIB-152
Raji B cells	ATCC	Cat# CCL-86
Oligonucleotides		
Primers for plasmid construction	This paper	Table S2
Recombinant DNA		
FGllF	This paper	N/A
pmCherry-N1	Clontech	Clontech plasmid # 632523
pEGFP-N1	Clontech	Clontech plasmid # 6085-1
pCMV-lyso-pHluorin	Addgene	Addgene plasmid # 70113
pMD2.G	Addgene	Addgene plasmid # 12259
psPAX2	Addgene	Addgene plasmid # 12260
pGEX-4T-1	Amersham	catalog # 27458001
pLentiCas9-blasticidin	Addgene	Addgene plasmid # 52962
pLentiguide-puro_hNKD2sg#1	This paper	Details in Table S2
pLentiguide-puro_hNKD2sg#2	This paper	Details in Table S2
pLentiguide-puro_hNKD2sg#3	This paper	Details in Table S2
pLentiguide-puro_hORAI1sg	This paper	Details in Table S2
MO70-C-FLAG-hNKD2	This paper	Details in Table S2
pEGFPN1-hNKD2	This paper	Details in Table S2
pcDNA3.1_hNKD2	This paper	Details in Table S2
FG11F-C-FLAG-hNKD2	This paper	Details in Table S2
pCDNA3.1-NKD2^{S31A}	This paper	Details in Table S2
pN1mcherry-NKD2^{S31A}	This paper	Details in Table S2
pN1mcherry-NKD2^{EFMUT}	This paper	Details in Table S2
pN1mcherry-NKD2^{G2A}	This paper	Details in Table S2
pEGFPC1-ORAI1-EC-HA	This paper	Details in Table S2
MO91-ORAI1^{N223A}-TEV-pHluorin (ORAI1-EC-pHluorin)	This paper	Details in methods below and Table S2

REAGENT or RESOURCE	SOURCE	IDENTIFIER
Software and algorithms		
Slidebook software	Intelligent Imaging Innovations, Inc.	N/A
OriginPro	Originlab	N/A
ImageJ	NIH	N/A
Fluoview FV10i Confocal Microscope	Olympus	N/A
Fluoview software	FlowJo, LLC	N/A
Other		
LAS-3000 LCD camera	FujiFilm	N/A
ECM 830 electroporator	BTX	N/A
BD Fortessa flow cytometer	BD Biosciences	N/A